

***In silico* identification of widely used and well tolerated drugs that may inhibit SARS-Cov-2 3C-like protease and viral RNA-dependent RNA polymerase activities, and may have potential to be directly used in clinical trials**

Seref Gul<sup>1</sup>, Onur Ozcan<sup>2</sup>, Sinan Asar<sup>3</sup>, Alper Okyar<sup>4</sup>, Ibrahim Baris<sup>2</sup>, Ibrahim Halil Kavakli<sup>1, 2\*</sup>

Departments of <sup>1</sup>Chemical and Biological Engineering, <sup>2</sup>Molecular Biology and Genetics, Koc University, Rumelifeneri Yolu, Sariyer, Istanbul, Turkey

<sup>3</sup>Department of Anesthesiology and Reanimation, Bakırköy Dr. Sadi Konuk Training and Research Hospital, University of Health Sciences, Istanbul, Turkey.

<sup>4</sup>Department of Pharmacology, Istanbul University Faculty of Pharmacy, TR-34116 Beyazit, Istanbul, Turkey

**\*Corresponding author**

İbrahim Halil Kavakli

Chemical and Biological Engineering

Koc University

Rumelifener Yolu

Sariyer, Istanbul

Turkey

Email: [hkavakli@ku.edu.tr](mailto:hkavakli@ku.edu.tr)

## **ABSTRACT**

Despite drastic strict measures, the spread of the SARS-CoV-2 is ongoing all around the world. There is no vaccine developed against this virus and no approved medication to be used for the treatment of COVID-2019. In this study, we performed *in silico* screening against two critical enzymes (3C-like protease (3CL<sup>pro</sup>) and viral RNA-dependent RNA polymerase (RdRp)), which play important roles in the SARS-CoV-2 life cycle, by using the U.S. Food and Drug Administration (FDA) approved drugs. Our docking simulations enable us to identify several hundred drugs that have high binding affinity for each target. To evaluate persistence of the drugs' binding to each target near to physiological conditions we selected well tolerated and widely used ones for the molecular dynamics simulations. Simulations results revealed that following drugs were stably interacting with SARS-Cov-2 3CL<sup>pro</sup>: tetracycline and its derivatives, dihydroergotamine, ergotamine, dutasteride, nelfinavir, and paliperidone. A similar analysis with RdRp showed that eltrombopag, tipranavir, ergotamine, and conivaptan were bound with the enzyme during the simulation with high binding energy. Detailed analysis of docking results suggested that ergotamine, dihydroergotamine, bromocriptine, dutasteride, conivaptan, paliperidone, and tipranavir can bind to both enzymes with high affinity. Since these drugs are well tolerated, cost effective and widely used, our study suggested that they have potential to be used in clinical trial for the treatment of SARS-CoV-2 infected patients.

**Keywords:** SARS-CoV-2, 3 Chymotrypsin like protease, RNA dependent RNA polymerase, drug repurposing, tetracycline, dutasteride

## 1. INTRODUCTION

Coronaviruses (CoVs) belong to a large family of viruses, which circulate among the animals like bats, camels and cats (Habibzadeh and Stoneman, 2020). CoVs, those have ability to transmit from animals to human, result serious upper respiratory tract diseases (Su et al., 2016). Such outbreaks, caused by the severe acute respiratory syndrome coronaviruses (SARS-CoVs), are observed in 2002 and 2003 in China (Drosten et al., 2003; Ksiazek et al., 2003). A decade later, Middle East Respiratory Syndrome coronavirus (MERS-CoV), another pathogenic coronavirus with a clinical picture reminiscent of SARS, was isolated in patients presenting with pneumonia in the Middle Eastern countries (Zaki et al., 2012). A novel coronavirus (SARS-nCoV-2) has appeared in Wuhan, China and has turned into a global health concern. Sequence analysis of the full-length genome of SARS-nCoV-2 showed 96% identity to a bat coronavirus (Wu et al., 2020; Zhou et al., 2020). Further amino acid comparison demonstrates that it is closer to the SARS-related coronaviruses (SARS-CoVs) compared to other type of CoVs. World Health Organization named diseases COVID-19 cause by 2019-nCoV (WHO, 2020).

SARS-nCoV-2 has linear (+) single-stranded RNA genomes and genes encodes for the same proteins like other family members (Wu C, 2020; Wu et al., 2020). Analyses of its genome organization comparing with other coronavirus members predicted RNA synthesis machinery and life cycle to be conserved. All coronaviruses consist of following genes: the replicase (Rep 1a and 1b), the spike (S), envelope (E), membrane (M), and nucleoprotein (N) (Graham et al., 2008; Habibzadeh and Stoneman, 2020; Ziebuhr, 2005). They also possess genes encoding nonstructural proteins placed between these genes in different position depending type of each virus (Gorbalenya et al., 2006). The replication of coronavirus in the cell starts by translating two overlapping open reading frames (ORF1a and ORF1b) (Scandella et al.,

2006; St John et al., 2015; Su et al., 2016; Ziebuhr, 2005). This produces pp1a and pp1ab, which generated by (-)1 ribosomal frameshift mechanism (Firth and Brierley, 2012). These polyproteins are proteolytically processed via two essential viral cysteine proteases, which are the papain-like protease (PL<sup>pro</sup>, or nsp3) and the 3C-like protease (3CL<sup>pro</sup>, also known as the main protease, M<sup>pro</sup>, or nsp5) (Thiel et al., 2003; Ziebuhr, 2004). Cleavage of polypeptides by both proteases results in the production of 16 nonstructural proteins (nsps) where PL<sup>pro</sup> is responsible for cleavage at 3 sites and 3CL<sup>pro</sup> is responsible for cleavage at 11 sites in a complex of non-structural proteins (Prajapat et al., 2020). The nsp12, which is the first protein encoded by ORF1b, has common viral RNA-dependent RNA polymerase (RdRp) motifs, and is thus the catalytic core of the RNA replicase (Xu et al., 2003). RdRp requires nsp7 and nsp8 co-factors to display maximal polymerase activity (Kirchdoerfer and Ward, 2019). This complex is responsible for transcribing both positive and negative strand of RNAs (Thiel et al., 2003).

The viral life cycle has multiple stages, including entry, replication of its genetic material, protein translation, assembly, and release. Throughout the entire process, many viral proteins and host receptors can be targeted for drug development. Given the crucial role of RdRp and 3CL<sup>pro</sup> in the virus life cycle and identifications of small molecules interfering enzymatic activities of either 3CL<sup>pro</sup> or RdRp or both in the treatment of SARS-nCoV-2 viral infections, are attractive targets.

There are different strategies or targets can be employed to interfere with life cycle of coronavirus life cycle (Li et al., 2020; Wu C, 2020). Thus, in the present study, we took *in silico* drug repurposing approach to find candidate molecule that may interfere with enzymatic activity of the SARS-Cov-2 3CL<sup>pro</sup> and RdRp by using library of FDA approved

drugs. Our studies revealed that 360 and 850 molecules have high affinity ( $<-7.5\text{kcal/mol}$ ) to SARS-Cov-2 3CL<sup>pro</sup> and RdRp, respectively. After the identification of the drugs that have potential to bind both viral enzymes, we performed detailed literature analysis to determine well tolerated drugs that were shown to have *in vitro* antiviral activity. We found several following drugs that have potential to be directly used clinical trial; chemotherapeutics (tetracycline and its derivatives), drugs for migraine headaches (ergotamine and dihydroergotamine), vasopressin receptor antagonist (conivaptan and tolvaptan), antiandrogen (dutasteride) and thrombopoietin receptor agonist (eltrombopag). Our results suggest that these drugs might be used alone or in combination as adjuvant with current protocols for the treatment of SARS-nCoV-2.

## **2. MATERIALS AND METHODS**

### **2.1 Protein and ligand preparation for docking simulations**

We initially performed pairwise multiple sequence alignment to determine the degree of conservation between SARS-CoV-2 and with other coronavirus family members for 3CL<sup>pro</sup> and RdRp using EMBL-EBI server (Madeira et al., 2019) and JalView (2.11.0). Then, initial structures for SARS-Coronavirus RdRp (PDB ID: 6NUR) and 3CL<sup>pro</sup> (PDB ID: 6Y84) were retrieved from The Protein Data Bank ([www.rcsb.org](http://www.rcsb.org)). Proteins were prepared for docking simulations via UCSF Chimera, Dock Prep module. Excess water molecules and, in case of presence of alternate locations for residues, the ones with the lower occupancies were removed from structures. Any missing side chains were completed by using the Dunbrack 2010 rotamer library. Polar hydrogens were added, non-polar hydrogens were merged with atoms that they are bound and finally Gasteiger charges were introduced to structures with Auto Dock Tools (ADT) suite. Structures of drugs were obtained from Zinc15 database

catalogue of FDA-approved drugs that are imported from the compounds within the U.S. Environmental Protection Agency's (EPA) Distributed Structure-Searchable Toxicity (DSSTox) database. The 3498 drugs and inhibitors of HKU4-CoV 3CL<sup>pro</sup> were prepared for docking by using Auto Dock Tools (ADT) suite. While previously identified active site of 3CL<sup>pro</sup> containing the catalytic dyad (Cys<sup>145</sup> and His<sup>41</sup> in SARS-CoV-2) was used as grid center for docking simulations of the protease, binding site of nsp8 protein was identified as the grid center for RdRp. All docking studies were performed via AutoDock Vina (version 1.1.2) (<http://vina.scripps.edu/>) (Trott and Olson, 2010).

## **2.2 Molecular dynamics simulations**

Protein structures were solvated in a rectangular box using TIP3P water molecules and neutralized with sodium and chloride ions and then additional 0.150 mM Na<sup>+</sup> Cl<sup>-</sup> ions were added to system by using visual molecular dynamics (VMD) program (Humphrey et al., 1996). Energy minimization was performed for 20,000 steps. Systems was gradually heated and equilibrated in NPT ensemble for 1,4 ns. Throughout equilibration, constrains on the proteins were gradually removed starting from 2 kcal/mol/Å<sup>2</sup>. After equilibration, a production run of 20 ns for each complex was performed. Time step was set to 2fs; van der Waals (12Å cut-off) and long-range electrostatic interactions (via particle-mesh Ewald) were included to calculate the force acting on the system. All production runs were performed at 310 K and under 1 atm pressure using a Langevin thermostat and a Langevin barostat, respectively. All simulations were performed by using NAMD (Phillips et al., 2005) software and CHARMM36m forcefield (Huang et al., 2017) on inhouse, local machines. The numerical calculations reported in this paper were partially performed at TUBITAK ULAKBIM, High Performance and Grid Computing Center (TRUBA resources). All analysis regarding the molecular dynamics simulations were performed using VMD with inhouse

scripts, and protein representations were prepared by using Pymol (DeLano, 2009). Parameters of drugs for molecular simulations were generated through CHARMM-GUI (Jo et al., 2008; Kim et al., 2017).

Molecular mechanics generalized born surface area (MM/GBSA) method is used to calculate binding free energy of drug to its target protein via MMPBSA.py script of AmberTools18 (D.A. Case, 2008). For each calculation, 1000 frames obtained from 20 ns simulation were used. 5 drugs repurposed to bind active site of 3CL<sup>pro</sup> and previously identified 3 inhibitors of 3CL<sup>pro</sup> were simulated and their binding free energies to protease were calculated. Similar analysis was done for 4 drugs repurposed to bind nsp8 binding site of RdRp.

### 3. RESULTS AND DISCUSSION

#### 3.1 Selection of target proteins

Different strategies are available to develop antiviral drugs such as blocking the virus binding to human cell receptors, inhibition of virus replication, or inhibition of virus's self-assembly process (Li et al., 2020; Wu C and Zheng M, 2020). The first attractive target for the development of anti-coronaviral therapeutics are the 3C-like protease (3CL<sup>pro</sup>) and RdRp (nsp12), which are essential for the progression of the coronaviral life cycle (Gorbalenya et al., 2006; Wu et al., 2020). The 3CL<sup>pro</sup> is required for cleavage of the nonstructural proteins and, in turn, controls the activities of replication complex (Anand et al., 2003). The second attractive target is RdRp, which is an essential enzyme in replication of viral RNA genome. Therefore, 3CL<sup>pro</sup> and RdRp were selected as drug target to screen U.S. Food and Drug Administration (FDA) approved drugs to identify molecules with low binding energy with pipeline indicated in **Figure 1**. Recently, the crystal structure of 3CL<sup>pro</sup> of the SARS-nCoV-2

has been released with PDB ID:6y84 (**Figure 2A**). Analysis the active site of 3CL<sup>pro</sup> of the 2019-nCoV revealed the conservation of catalytic dyad (Cys<sup>148</sup> and His<sup>41</sup>) between SARS-CoV, MERS-CoV, and HUK4 (**Figure 2B**). Further comparison of SARS-CoV-2 crystal structure with other members of CoVs indicated the high similarity between the folds (**Figure 2C**) (Anand et al., 2003; Tomar et al., 2015). The experimental verification of the active site was further confirmed by developing inhibitory molecules binding the active sites of 3CL<sup>pro</sup> for SARS-CoV (St John et al., 2015).

The RdRp (nsp12) needs to associate with nsp7 and nsp8 to exhibit maximal activity. The crystal structure of SARS-CoV nsp12 with nsp7 and nsp8 has been solved (Kirchdoerfer and Ward, 2019). This enabled us to identify the critical region of the RdRp that interacts with cofactor of nsp8 (**Figure 3A**).

Therefore, we targeted this interaction site, which also conserved in 2019-CoV (**Figure 3B**), to carry out *in silico* screening. We reasoned that molecules might inhibit the interaction between RdRp (nsp12) and nsp8 and, then interferes with replisome activity of the nsp12. Thus, these drugs may be used as in antiviral therapies.

### 3.2 Strategy of Identification of Candidates Drugs

The library was prepared by collecting 3948 FDA approved drugs from commercially available ZINC database (<http://zinc15.docking.org/catalogs/fda>) (Irwin and Shoichet, 2005). Virtual screening was performed as described previously (Armutlu et al., 2009; Doruk et al., 2020). For molecular docking simulations, AutoDock Vina is used to predict the optimal conformations of the receptor-ligand complex and report binding affinity scores by assuming a structure model with a rigid receptor (protein) and a flexible ligand. In the present study, to determine a cut off value for binding energies of drugs to 3CL<sup>pro</sup>, we first calculated the

binding energies of the previously identified inhibitors to HKU4-CoV 3CL<sup>pro</sup> (St John et al., 2015). The binding energies of these inhibitors (4f4, rfm, 4f5) were from -7.5 kcal/mol to -7.0 kcal/mol (Table 1). Therefore, we set -7.5 kcal/mol as cut off value. Histogram of Vina binding affinity of all drugs used in this study given in supplementary (Figure S1). Although docking simulations, *per se*, are utilized to identify strongly binding ligands to protein of interest, interactions captured in docking may be transient. Molecular dynamics simulation of biomolecules which allows to monitor dynamics of a system throughout a certain period of time is a versatile tool to evaluate the persistency of interaction between ligand and protein. To test and verify the stability of interaction between selected drugs and proteins we run 20ns molecular dynamics simulations. For drugs that kept the docking position and interacted with protein throughout the simulation binding free energy between drugs and protein via MM/GBSA method was calculated.

### **3.3 Docking and molecular dynamic simulation of tested drugs against SARS-Cov-2 3C-like protease**

Among screened 3948 FDA approved drugs, 360 molecules have docking scores better than -7.5 kcal/mol for SARS-Cov-2 3CL<sup>pro</sup> (top 100 were listed in Table S1). Top 15 hit compounds with <-8.6 kcal/mol are shown in Table 1. Docking analysis suggested that clinical drugs with antiviral, antibacterial, anticancer, and analgesic effects have high affinity to SARS-Cov-2 3CL<sup>pro</sup>. Among these, the following drugs are widely used and well tolerated: tetracycline and its derivatives, dutasteride, ergotamine, dihydroergotamine, bromocriptine, nelfinavir, and paliperidone.

*in-silico* analyses revealed that tetracyclines which are well known broad-spectrum semisynthetic antibiotics have high affinity to SARS-Cov-2 3CL<sup>pro</sup>. Our analysis showed both

tetracycline (-8.1 kcal/mol) and following derivatives binds to SARS-Cov-2 3CL<sup>pro</sup> with high affinity: metacycline (-9.1 kcal/mol), doxycycline (-8.2 kcal/mol), oxytetracycline (-8.5 kcal/mol), rolitetracycline (-8.2 kcal/mol), chlortetracycline (-8.2 kcal/mol), and tigecycline (-6.9 kcal/mol). Inspection of docking pose of tetracycline shows that drug occupies the catalytic site of SARS-Cov-2 3CL<sup>pro</sup> and interacts with catalytically active His<sup>41</sup> and Cys<sup>145</sup> residues (**Figure 4A**). In addition, drug is interacting with polar residues (Ser<sup>46</sup>, Asn<sup>142</sup>, and Glu<sup>166</sup>) around the active site of SARS-Cov-2 3CL<sup>pro</sup> and produce several H-bond interactions through Ser<sup>46</sup> and Glu<sup>166</sup>. Complete list of interacting residues of tetracycline are given in Table 2. Analysis of molecular dynamics simulations indicated that these interactions are very well maintained through the entire simulation (**Figure 4A**). In addition, mostly conserved interactions between tetracycline and Met<sup>49</sup> and Gln<sup>189</sup> during the simulation suggest that tetracycline stably interacts with the catalytic site of SARS-CoV-2 3CL<sup>pro</sup> and may inhibit the protease activity. Notably, several *in vitro* screening studies, doxycycline showed antiviral activity and significantly inhibited vesicular stomatitis virus (VSV), porcine reproductive and respiratory syndrome virus (PRRSV), and dengue viruses (DENV1-4) replication (Li et al., 2017; Rothan et al., 2014a; Wu et al., 2015) (Rothan et al., 2013; Rothan et al., 2014b). These suggest that doxycycline may have broader activity in inhibiting viral replication, in addition to its well-defined bacteriostatic activity. Doxycycline is well tolerated, has great distribution to tissues, and has a bioavailability of over 80% when taken orally (Agwuh and MacGowan, 2006; Smilack, 1999). In a recent *in silico* study, other tetracycline derivatives (doxycycline, oxytetracycline, and tigecycline) were reported to have high binding affinity to 3CL<sup>pro</sup> (Wu C and Zheng M, 2020).

Secondly, ergotamine and its derivatives dihydroergotamine and bromocriptine were found to have high bind affinity to SARS-Cov-2 3CL<sup>pro</sup>. Ergotamine is an alpha-1 selective adrenergic

agonist and is commonly used in the treatment of migraine disorders (Silberstein, 1997). Ergotamine has high docking binding energy against SARS-Cov-2 3CL<sup>pro</sup> with -8.6 kcal/mol. Similarly, dihydroergotamine is a 9,10- $\alpha$ -dihydro derivative of ergotamine and showed high affinity with -8.6 kcal/mol. Dihydroergotamine binds to SARS-Cov-2 3CL<sup>pro</sup> in a U-shaped form in docking simulations (**Figure 4B**). Analysis of interacting residues shows that dihydroergotamine interacts with catalytically active His<sup>41</sup> and Cys<sup>145</sup> residues and with polar residues (Thr<sup>25</sup>, Thr<sup>26</sup>, Ser<sup>46</sup> and Glu<sup>166</sup>) and forms H-bonds with Thr<sup>25</sup> and Glu<sup>166</sup> surrounding the active site of 3CL<sup>pro</sup> (list of interacting residues given in Table 2). Molecular dynamics simulations showed the stability of interaction between dihydroergotamine and the protease. Interactions suggested by docking were verified by molecular dynamics simulation in which critical interactions between drug and Thr<sup>25</sup>, His<sup>41</sup>, Met<sup>49</sup>, and Ser<sup>46</sup> residues are mostly conserved during the simulation (**Figure 4B**). The double-blind, randomized, placebo-controlled, parallel-group multi center studies revealed that this commonly used drugs are well tolerated, and the adverse events were generally mild or moderate, and transient (Christie et al., 2003; Diener et al., 2002). However, it is not advised to combine ergotamine with protease inhibitors such as nelfinavir and indinavir because of interaction potential through CYP3A4 an isoform cytochrome P-450 enzyme (Mortier et al., 2001; Rosenthal et al., 1999).

Bromocriptine is an another semisynthetic ergot alkaloid derivative and functions as a dopamine receptor agonist and serotonin modulator (Kvernmo et al., 2006). Clinically, bromocriptine is used to treat hyperprolactinemia and Parkinson's disease (Kvernmo et al., 2006; Via et al., 2010). Bromocriptine showed high binding affinity against both RdRp and SARS-Cov-2 3CL<sup>pro</sup> with -9.2 kcal/mol and -8.6kcal/mol, respectively. Several in vitro and in vivo studies showed that bromocriptine inhibited Zika virus NS2B-NS3 protease activity,

and interfered with Dengue virus post-translation and/or RNA synthesis steps via NS3 (Chan et al., 2017; Kato et al., 2016; Yuan et al., 2017).

Dutasteride is an oral synthetic 4-azasteroid, and blocks type I and II 5 $\alpha$ -reductase enzymes and cause antiandrogenic activity. Type I and II 5 $\alpha$ -reductase enzymes convert testosterone into dihydrotestosterone (DHT), a primary hormonal mediator that plays a role in the development and enlargement of the prostate gland (Andriole and Kirby, 2003; Clark et al., 2004). Dutasteride was approved by the FDA in 2001 for the treatment of symptomatic benign prostatic hyperplasia (BPH). Large open-label extension studies continued for at least 2 years revealed that dutasteride is well-tolerated and drug-related adverse events were reported in less than 2% of patients (Marberger, 2006; Roehrborn et al., 2002; Thomson, 2005). Docking analyses revealed that dutasteride has high docking binding energy against SARS-Cov-2 3CL<sup>pro</sup> with -8.9 kcal/mol (**Figure 4C**).

Nelfinavir is an HIV-1 protease inhibitor drug used in the treatment of the human immunodeficiency virus (HIV). The binding energy of nelfinavir to target was calculated as -8.6 kcal/mol (**Figure 4D**). Interestingly, Yamamoto and his colleagues showed that nelfinavir, strongly inhibited replication of the SARS coronavirus (SARS-CoV) (Yamamoto et al., 2004). Nelfinavir inhibited the cytopathic effect induced by SARS-CoV infection. It is known that nelfinavir and other protease inhibitors are well tolerated and can be a good choice in treatment of SARS-CoV-2 infection.

Binding poses of dutasteride and nelfinavir in docking simulations show some similarities. In addition to binding to aforementioned polar residues interacting with tetracycline and dihydroergotamine, 1,4-bis(trifluoromethyl) benzene and benzyl moieties of dutasteride and

nelfinavir, respectively, stack to a hollow between Gln<sup>189</sup> and Pro<sup>68</sup> which stabilizes the interaction between drugs and the protease. While dutasteride make H-bond interactions with Thr<sup>25</sup> and Glu<sup>166</sup>, nelfinavir can only make such an interaction with Glu<sup>166</sup> (**Figure 4C, D**) (Table 2). Molecular dynamics simulations show that interaction with Cys<sup>145</sup> and Glu<sup>166</sup> for dutasteride; His<sup>41</sup> and Glu<sup>166</sup> for nelfinavir are very well maintained. These observations show that these two drugs can strongly interact with the active site of 3CL<sup>pro</sup> and inhibit its activity.

Paliperidone is an oral antipsychotic for the treatment of schizophrenia (Janicak and Winans, 2007). Three 6-week trials in patients with acute schizophrenia reported that extended release form of paliperidone ER was effective and well tolerated, compared with placebo (Davidson et al., 2006; Marder et al., 2007). It undergoes limited hepatic metabolism, thereby minimizing the risks of hepatic drug–drug and drug–disease interactions (Janicak and Winans, 2007). Paliperidone showed high binding affinity against both 3CL<sup>pro</sup> and RdRp with -8.8 kcal/mol and -8.6 kcal/mol, respectively. Similar to dihydroergotamine, paliperidone binds to 3CL<sup>pro</sup> in a U-shaped conformation and interact with polar residues Thr<sup>25</sup>, His<sup>41</sup>, Ser<sup>46</sup>, and Gln<sup>189</sup> (**Figure 4E**). Other than these, interactions between paliperidone and 3CL<sup>pro</sup> are hydrophobic. Consistent with interactions observed in docking conformation, paliperidone interacts with these polar residues almost through the entire simulation (**Figure 4E**).

Molecular dynamics simulations of selected drugs with SARS-Cov-2 3CL<sup>pro</sup> show that interactions between these drugs and the protease are stable which suggests that selected drugs are promising candidates to inhibit SARS-Cov-2 3CL<sup>pro</sup> activity. Furthermore, we calculated binding free energy of selected drugs to the protease by using MM/GBSA method to assess their binding strength from these MD simulations. As controls we simulated 4f4 and 4f5 molecules which were previously identified as 3CL<sup>pro</sup> inhibitors and calculated their binding free energies to 3CL<sup>pro</sup> (Table 3) (Figure S2). While 4f4 and 4f5 have binding free

energy of -16.71 kcal/mol and -24.96 kcal/mol, respectively. Tetracycline, dihydroergotamine, dutasteride, nelfinavir, and paliperidone have binding free energy of -14.6, -16.22, -20.47, -26.28, and -18.23 kcal/mol, respectively (Table 3). Comparable or better binding free energy values of selected drugs with inhibitors indicate that these drugs have high potential to interfere with the activity of 3CL<sup>pro</sup> activity in SARS-CoV-2.

Interestingly, seven of top 20 drugs have cytostatic activity and are used in cancer therapy: irinotecan, etoposid, teniposide, doxorubicin, epirubicin and proscillaridin. Although it seems unrelated, it is well known that HIV protease inhibitors showed anticancer activity via two main mechanisms; endoplasmic reticulum stress-unfolded protein response pathway and Akt inhibition (Gantt et al., 2013; Maksimovic-Ivanic et al., 2017). Expectedly, nelfinavir was shown to have *in vitro* anticancer activity as well (Gantt et al., 2013). The HIV protease inhibitors including nelfinavir and lopinavir are peptidomimetics and those drugs with similar structures are expected to bind nelfinavir docking site in 3CL<sup>pro</sup>. Although several anticancer drugs displayed *in silico* interaction with 3CL<sup>pro</sup> ( $\leq -8.6$  kcal/mol), the use of this kind of molecules as antivirals may not be recommended due to their serious adverse or toxic effects.

### **3.4 Docking and molecular dynamic simulation of tested drugs against RNA-dependent RNA polymerase**

Docking analyses revealed 850 drugs with docking binding energies  $< -7.5$  kcal/mol against nsp8 binding sites of RdRp (top 100 drugs are listed in Table S2). Top 15 hit compounds with  $< -9.2$  kcal/mol are shown in Table 4. Among them, we identified the following drugs that are well tolerated and widely used, and have high binding affinity against RdRp; ergotamine, dihydroergotamine, bromocriptine, tipranavir, conivaptan, and eltrombopag.

Notably, ergotamine and its derivatives dihydroergotamine and bromocriptine showed high affinity against RdRp with -9.8 kcal/mol, -9.3 kcal/mol, and -9.2 kcal/mol respectively. As explained above, these drugs showed high binding affinity (<-8.6 kcal/mol) against 3CL<sup>pro</sup>. Binding mode of ergotamine showed that drug establishes several H-bond interactions with backbone oxygen atoms of Thr<sup>324</sup>, Phe<sup>326</sup> and Pro<sup>328</sup>. In addition, ergotamine interacts with RdRp via hydrophobic interactions as well (**Figure 5A**). Complete list of ergotamine interacting residues were given in Table 5. To examine dynamic interactions between ergotamine and RdRp we run 20ns simulations of RdRp docked with ergotamine. Molecular dynamics simulation showed that interaction between the drug and Thr<sup>324</sup>, Pro<sup>328</sup>, and Val<sup>398</sup> were mostly carried on (**Figure 5A**). Conservation of these interactions through the simulation indicates that ergotamine has high affinity to RdRp. Thus, our results make ergotamine and dihydroergotamine as a candidate for further *in vitro* and clinical evaluation of anti-SARS-CoV-2 activity.

Eltrombopag is a human thrombopoietin receptor agonist which is used to treat low blood platelet counts in adults with chronic immune (idiopathic) thrombocytopenia (ITP) (Erickson-Miller et al., 2009). The metabolism and disposition of eltrombopag were studied in six healthy men after a single oral administration of a solution dose of [(<sup>14</sup>C)] eltrombopag (75 mg, 100  $\mu$ Ci). Eltrombopag was well tolerated (Deng et al., 2011). Eltrombopag was shown *in vitro* to inhibit SFTS virus replication. This retrovirus causes severe fever with thrombocytopenia syndrome (SFTS) which is a newly recognized viral hemorrhagic fever and has emerged in rural areas of China and then in Japan and South Korea (Yu et al., 2011). In a recent *in vitro* screening study, eltrombopag was shown to have antiviral activity against SARS-CoV-2 with IC<sub>50</sub> value <10  $\mu$ M (Jeon et al., 2020). In our docking simulation

eltrombopag was one of the best drugs having high binding affinity (-9.5 kcal/mol) to RdRp. Docking position showed that multiple H-bonds are established between drug and the polymerase. For example, backbone oxygen atoms of Thr<sup>324</sup>, Pro<sup>328</sup>, and Leu<sup>329</sup> and hydrogen atoms on side chain of Arg<sup>331</sup> are in H-bond distance with their interacting partners on eltrombopag (**Figure 5B**). In addition, Val<sup>330</sup> and Val<sup>398</sup> make hydrophobic interaction with the drug. Conservation of all these polar and hydrophobic interactions throughout the molecular dynamics simulation indicate that eltrombopag can stably bind to nsp8 binding site of RdRp (**Figure 5B**). Additionally, eltrombopag showed high binding affinity against 3CL<sup>pro</sup> with -8.2 kcal/mol.

Conivaptan is a non-peptide inhibitor of antidiuretic hormone arginine vasopressin (AVP) V<sub>1A</sub> and V<sub>2</sub> receptors. Conivaptan showed high binding affinity against both RdRp and 3CL<sup>pro</sup> with -9.4 kcal/mol and -8.7 kcal/mol, respectively. Docking position of conivaptan suggest that while most interactions with RdRp are hydrophobic, backbone oxygen atoms of Leu<sup>270</sup> and Val<sup>330</sup> interact with drug via H-bond interactions (**Figure 5C**) (Table 5). Molecular dynamics simulations showed that interactions with these two residues are mostly maintained throughout the simulation. In addition, Thr<sup>324</sup> and Val<sup>398</sup> interactions are very well kept as well (**Figure 5C**). Conivaptan inhibits both isotypes of the vasopressin receptor (V<sub>1a</sub> and V<sub>2</sub>) and used for the treatment of euvolemic or hypervolemic hyponatremia (e.g. the syndrome of inappropriate secretion of antidiuretic hormone, or in the setting of hypothyroidism, adrenal insufficiency, pulmonary disorders, etc.) in hospitalized patients. The placebo-controlled, randomized, double-blind multicenter studies revealed that oral conivaptan is well tolerated in cases with hyponatremia (Annane et al., 2009; Ghali et al., 2006). Montes-Grajales et al. (2020) performed *in silico* and *in vitro* analyses and reported that conivaptan showed some antiviral activity against dengue (DENV) and Zika (ZIKV) viruses at high concentrations

( $IC_{50} > 100 \mu M$ ). Another AVP receptor 2 antagonist, tolvaptan, has also high binding affinity against RdRp with  $-9.2 \text{ kcal/mol}$ . Similarly, tolvaptan is used to treat low blood sodium levels (hyponatremia) associated with various conditions (Montes-Grajales et al., 2020).

Tipranavir is a sulfonamide-containing dihydropyrene and a nonpeptidic protease inhibitor that targets the HIV protease. Interestingly, Tipranavir has high affinity against not only to 3CL<sup>pro</sup> but also to RdRp with  $-8.4 \text{ kcal/mol}$  and  $-9.3 \text{ kcal/mol}$ , respectively. Binding mode of tipranavir to RdRp suggests that drug forms a H-bond interaction with backbone oxygen atom of Leu<sup>271</sup>. In addition, fluorine atoms on trifluoromethylpyridine moiety of tipranavir are in H-bond distance with Arg<sup>331</sup> (**Figure 5D**). Val<sup>330</sup>, Phe<sup>396</sup>, and Val<sup>398</sup> residues enable to establish hydrophobic interaction between the drug and RdRp (Table 5). While these hydrophobic interactions are mostly maintained in molecular dynamics simulations, interaction with Leu<sup>271</sup> and Arg<sup>331</sup> are not conserved especially after first 5 ns of the simulation. Instead the drug started to interact more frequently with Thr<sup>324</sup> and Leu<sup>389</sup>. These changes and conservations in the interaction pattern of tipranavir shows that as the simulation progress despite some changes in interacting residues, tipranavir is still very close to initial docking position and may disrupt nsp8 binding.

Finally, binding free energies of selected drugs to RdRp were calculated by using MM/GBSA method. Although we do not have a reference molecule to compare the binding free energies, the values calculated for 3CL<sup>pro</sup> give an idea that binding free energies around  $-20 \text{ kcal/mol}$  can be accepted as high affinity of drugs to target protein. Our calculations showed that ergotamine, eltrombopag, conivaptan, and tipranavir have binding energies of  $-24.65$ ,  $-35.33$ ,  $-23.85$ , and  $-26.08 \text{ kcal/mol}$ , respectively, to the RdRp. All docking and molecular dynamics simulations analyses indicate that ergotamine, dihydroergotamine, eltrombopag, conivaptan

and tipranavir are strong candidates to bind to nsp8 binding site of RdRp in which they can prevent nsp8 binding. If that is case, using these molecules in therapies can attenuate the maximum RdRp activity in SARS-CoV-2.

We further validate our results with docking other antiviral drugs lopinavir and ritonavir. Results indicated that both drugs have a docking score with -7.7 kcal/mol and -6.8 kcal/mol against 3CL<sup>pro</sup>, respectively. Lopinavir and ritonavir are anti-retroviral protease inhibitors used in combination with other antiretrovirals in the treatment of HIV-1 infection. Like many other protease inhibitors (e.g. nelfinavir), lopinavir and ritonavir are a peptidomimetic molecule. *In vitro* studies have shown that lopinavir and ritonavir combination can inhibit the replication of MERS-CoV and SARS-CoV to exert antiviral effects (Dyall et al., 2017).

#### **4. CONCLUSION**

Our *in-silico* analyses revealed that tetracyclines which are well known chemotherapeutics have high affinity to 3CL<sup>pro</sup>. This chemotherapeutics are cheap, well tolerated, and the patients may benefit not only their antibacterial and anti-inflammatory effects but also their antiviral activity. Secondly, dutasteride showed high affinity against 3CL<sup>pro</sup>. Dutasteride was shown to down regulate the expression of TMPRSS2 (Lucas et al., 2008; Mostaghel et al., 2014). It was recently shown that SARS-CoV-2 uses the ACE2 for entry and the serine protease TMPRSS2 for S protein priming. SARS-CoV-2 cell entry was blocked by TMPRSS2 protease inhibitor (Hoffmann et al., 2020). Thus, the patients may benefit from dutasteride because of its effect on TMPRSS2 expression and its possible antiviral activity. Additionally, ergotamine, dihydroergotamine, bromocriptine conivaptan, eltrombopag, paliperidone, and tipranavir have strong interactions with both 3CL<sup>pro</sup> and RdRp, are also among the most promising candidates (Table S3). Since these drugs are cost-effective and widely used, they can be utilized alone or

in combination as an adjuvant with currently used protocols in the treatment of SARS-CoV-2 infection. Additionally, each of the above drugs can be used in different groups of patients because of their primary effects. For example, dutasteride might be used only in males because of its antiandrogenic effects. Eltrombopag can be used to alleviate thrombocytopenia observed in some patients. Since these drugs have high affinity to both target proteins, it could make the mechanism of action of these compounds less sensitive to variations of the SARS-CoV-2 3CL<sup>pro</sup> and RdRp proteins, which as is known, might led to the emergence of resistant strains. Because of their target proteins, the above drugs will exert their antiviral effect at the early–mid stage of infection, suggesting that it did not interfere with SARS-CoV-2 infectivity, adsorption, or entry into target cells.

When the literature was reviewed, we have found supportive *in vitro* findings for the antiviral activity of above listed drugs, encouraging us to take further steps. In a current scenario where no approved therapeutics and vaccines for SARS-CoV-2 infection is available, *in-silico* repurposing of approved drugs targeting viral proteins still represents a promising approach for discovering new antiviral molecules. Although the results of *in-silico* analysis must be confirmed with *in vitro* studies and clinical testing, the trials of commonly used, well tolerated drugs can be a good choice in immediate urgent situation.

### **Acknowledgments**

We would like to thanks to Drs Ahmet Gül and Mustafa Oral from Istanbul University School of Medicine their useful discussions.

### **Conflict of Interest**

Authors declare no conflict of interest.

## References

- Agwuh, K.N., MacGowan, A., 2006. Pharmacokinetics and pharmacodynamics of the tetracyclines including glycylicyclines. *J Antimicrob Chemother* 58, 256-265.
- Anand, K., Ziebuhr, J., Wadhvani, P., Mesters, J.R., Hilgenfeld, R., 2003. Coronavirus main proteinase (3CLpro) structure: basis for design of anti-SARS drugs. *Science* 300, 1763-1767.
- Andriole, G.L., Kirby, R., 2003. Safety and tolerability of the dual 5 alpha-reductase inhibitor dutasteride in the treatment of benign prostatic hyperplasia. *Eur Urol* 44, 82-88.
- Annane, D., Decaux, G., Smith, N., Grp, C.S., 2009. Efficacy and Safety of Oral Conivaptan, a Vasopressin-Receptor Antagonist, Evaluated in a Randomized, Controlled Trial in Patients With Euvolemic or Hypervolemic Hyponatremia. *Am J Med Sci* 337, 28-36.
- Armutlu, P., Ozdemir, M.E., Ozdas, S., Kavakli, I.H., Turkay, M., 2009. Discovery of Novel CYP17 Inhibitors for the Treatment of Prostate Cancer with Structure-Based Drug Design. *Lett Drug Des Discov* 6, 337-344.
- Chan, J.F., Chik, K.K., Yuan, S., Yip, C.C., Zhu, Z., Tee, K.M., Tsang, J.O., Chan, C.C., Poon, V.K., Lu, G., Zhang, A.J., Lai, K.K., Chan, K.H., Kao, R.Y., Yuen, K.Y., 2017. Novel antiviral activity and mechanism of bromocriptine as a Zika virus NS2B-NS3 protease inhibitor. *Antiviral Res* 141, 29-37.
- Christie, S., Gobel, H., Mateos, V., Allen, C., Vrijens, F., Shivaprakash, M., Pr, R.E.C., 2003. Crossover comparison of efficacy and preference for rizatriptan 10 mg versus ergotamine/caffeine in migraine. *Eur Neurol* 49, 20-29.
- Clark, R.V., Hermann, D.J., Cunningham, G.R., Wilson, T.H., Morrill, B.B., Hobbs, S., 2004. Marked suppression of dihydrotestosterone in men with benign prostatic hyperplasia by dutasteride, a dual 5alpha-reductase inhibitor. *J Clin Endocrinol Metab* 89, 2179-2184.
- D.A. Case, I.Y.B.-S., S.R. Brozell, D.S. Cerutti, T.E. Cheatham, III, V.W.D. Cruzeiro, T.A. Darden, R.E. Duke, D. Ghoreishi, M.K. Gilson, H. Gohlke, A.W. Goetz, D. Greene, R Harris, N. Homeyer, S. Izadi, A. Kovalenko, T. Kurtzman, T.S. Lee, S. LeGrand, P. Li, C. Lin, J. Liu, T. Luchko, R. Luo, D.J. Mermelstein, K.M. Merz, Y. Miao, G. Monard, C. Nguyen, H. Nguyen, I. Omelyan, A. Onufriev, F. Pan, R. Qi, D.R. Roe, A. Roitberg, C. Sagui, S. Schott-Verdugo, J. Shen, C.L. Simmerling, J. Smith, R. Salomon-Ferrer, J. Swails, R.C. Walker, J. Wang, H. Wei, R.M. Wolf, X. Wu, L. Xiao, D.M. York and P.A. Kollman 208. *AMBER 2018*. University of California, San Francisco.
- Davidson, M., Emsley, R., Kramer, M., Ford, L., Gassmann-Mayer, C., Lim, P., Pan, J., Eerdeken, M., 2006. Efficacy, safety and effect on functioning of oral paliperidone extended-release tablets in the treatment of acute schizophrenia: An International 6-week placebo-controlled study. *Schizophr Res* 81, 43-43.
- DeLano, W.L., 2009. PyMOL molecular viewer: Updates and refinements. *Abstr Pap Am Chem S* 238.
- Deng, Y., Madatian, A., Wire, M.B., Bowen, C., Park, J.W., Williams, D., Peng, B., Schubert, E., Gorycki, F., Levy, M., Gorycki, P.D., 2011. Metabolism and disposition of eltrombopag, an oral, nonpeptide thrombopoietin receptor agonist, in healthy human subjects. *Drug Metab Dispos* 39, 1734-1746.
- Diener, H.C., Jansen, J.P., Reches, A., Pascual, J., Pitei, D., Steiner, T.J., St, E.C.C., 2002. Efficacy, tolerability and safety of oral eletriptan and ergotamine plus caffeine (Cafergot (R)) in the acute treatment of migraine: A multicentre, randomised, double-blind, placebo-controlled comparison. *Eur Neurol* 47, 99-107.
- Doruk, Y.U., Yarparvar, D., Akyel, Y.K., Gul, S., Taskin, A.C., Yilmaz, F., Baris, I., Ozturk, N., Turkay, M., Ozturk, N., Okyar, A., Kavakli, I.H., 2020. A CLOCK-binding small molecule disrupts the interaction between CLOCK and BMAL1 and enhances circadian rhythm amplitude. *J Biol Chem* 295, 3518-3531.
- Drosten, C., Gunther, S., Preiser, W., van der Werf, S., Brodt, H.R., Becker, S., Rabenau, H., Panning, M., Kolesnikova, L., Fouchier, R.A., Berger, A., Burguiere, A.M., Cinatl, J., Eickmann, M., Escriou, N., Grywna, K., Kramme, S., Manuguerra, J.C., Muller, S., Rickerts, V., Sturmer, M., Vieth, S., Klenk, H.D., Osterhaus, A.D., Schmitz, H., Doerr, H.W., 2003. Identification of a novel coronavirus in patients with severe acute respiratory syndrome. *N Engl J Med* 348, 1967-1976.

Dyall, J., Gross, R., Kindrachuk, J., Johnson, R.F., Olinger, G.G., Hensley, L.E., Frieman, M.B., Jahrling, P.B., 2017. Middle East Respiratory Syndrome and Severe Acute Respiratory Syndrome: Current Therapeutic Options and Potential Targets for Novel Therapies. *Drugs* 77, 1935-1966.

Erickson-Miller, C.L., Delorme, E., Tian, S.S., Hopson, C.B., Landis, A.J., Valoret, E.I., Sellers, T.S., Rosen, J., Miller, S.G., Luengo, J.I., Duffy, K.J., Jenkins, J.M., 2009. Preclinical activity of eltrombopag (SB-497115), an oral, nonpeptide thrombopoietin receptor agonist. *Stem Cells* 27, 424-430.

Firth, A.E., Brierley, I., 2012. Non-canonical translation in RNA viruses. *J Gen Virol* 93, 1385-1409.

Gantt, S., Casper, C., Ambinder, R.F., 2013. Insights into the broad cellular effects of nelfinavir and the HIV protease inhibitors supporting their role in cancer treatment and prevention. *Curr Opin Oncol* 25, 495-502.

Ghali, J.K., Koren, M.J., Taylor, J.R., Brooks-Asplund, E., Fan, K., Long, W.A., Smith, N., Grp, C.S., 2006. Efficacy and safety of oral conivaptan: A V-1A/V-2 vasopressin receptor antagonist, assessed in a randomized, placebo-controlled trial in patients with euvolemic or hypervolemic hyponatremia. *J Clin Endocr Metab* 91, 2145-2152.

Gorbalenya, A.E., Enjuanes, L., Ziebuhr, J., Snijder, E.J., 2006. Nidovirales: evolving the largest RNA virus genome. *Virus Res* 117, 17-37.

Graham, R.L., Sparks, J.S., Eckerle, L.D., Sims, A.C., Denison, M.R., 2008. SARS coronavirus replicase proteins in pathogenesis. *Virus Res* 133, 88-100.

Habibzadeh, P., Stoneman, E.K., 2020. The Novel Coronavirus: A Bird's Eye View. *Int J Occup Environ Med* 11, 65-71.

Hoffmann, M., Kleine-Weber, H., Schroeder, S., Kruger, N., Herrler, T., Erichsen, S., Schiergens, T.S., Herrler, G., Wu, N.H., Nitsche, A., Muller, M.A., Drosten, C., Pohlmann, S., 2020. SARS-CoV-2 Cell Entry Depends on ACE2 and TMPRSS2 and Is Blocked by a Clinically Proven Protease Inhibitor. *Cell*.

Huang, J., Rauscher, S., Nawrocki, G., Ran, T., Feig, M., de Groot, B.L., Grubmuller, H., MacKerell, A.D., Jr., 2017. CHARMM36m: an improved force field for folded and intrinsically disordered proteins. *Nat Methods* 14, 71-73.

Humphrey, W., Dalke, A., Schulten, K., 1996. VMD: visual molecular dynamics. *J Mol Graph* 14, 33-38, 27-38.

Irwin, J.J., Shoichet, B.K., 2005. ZINC--a free database of commercially available compounds for virtual screening. *J Chem Inf Model* 45, 177-182.

Janicak, P.G., Winans, E.A., 2007. Paliperidone ER: a review of the clinical trial data. *Neuropsychiatr Dis Treat* 3, 869-897.

Jeon, S., Ko, M., Lee, j., Choi, I., Young Byun, S., Park, S., Shum, D., Kim, S., 2020. Identification of antiviral drug candidates against SARS-CoV-2 from FDA-approved drugs. <https://doi.org/10.1101/2020.03.20.999730>.

Jo, S., Kim, T., Iyer, V.G., Im, W., 2008. CHARMM-GUI: a web-based graphical user interface for CHARMM. *J Comput Chem* 29, 1859-1865.

Kato, F., Ishida, Y., Oishi, S., Fujii, N., Watanabe, S., Vasudevan, S.G., Tajima, S., Takasaki, T., Suzuki, Y., Ichiyama, K., Yamamoto, N., Yoshii, K., Takashima, I., Kobayashi, T., Miura, T., Igarashi, T., Hishiki, T., 2016. Novel antiviral activity of bromocriptine against dengue virus replication. *Antiviral Res* 131, 141-147.

Kim, S., Lee, J., Jo, S., Brooks, C.L., 3rd, Lee, H.S., Im, W., 2017. CHARMM-GUI ligand reader and modeler for CHARMM force field generation of small molecules. *J Comput Chem* 38, 1879-1886.

Kirchdoerfer, R.N., Ward, A.B., 2019. Structure of the SARS-CoV nsp12 polymerase bound to nsp7 and nsp8 co-factors. *Nat Commun* 10, 2342.

Ksiazek, T.G., Erdman, D., Goldsmith, C.S., Zaki, S.R., Peret, T., Emery, S., Tong, S., Urbani, C., Comer, J.A., Lim, W., Rollin, P.E., Dowell, S.F., Ling, A.E., Humphrey, C.D., Shieh, W.J., Guarner, J., Paddock, C.D., Rota, P., Fields, B., DeRisi, J., Yang, J.Y., Cox, N., Hughes, J.M., LeDuc, J.W., Bellini, W.J., Anderson, L.J., Group, S.W., 2003. A novel coronavirus associated with severe acute respiratory syndrome. *N Engl J Med* 348, 1953-1966.

Kvernmo, T., Hartter, S., Burger, E., 2006. A review of the receptor-binding and pharmacokinetic properties of dopamine agonists. *Clin Ther* 28, 1065-1078.

Li, H., Zhou, Y., Zhang, M., Wang, H., Zhao, Q., Liu, J., 2020. Updated approaches against SARS-CoV-2. *Antimicrob Agents Chemother*.

Li, Y.M., Wu, Z.C., Liu, K., Qi, P.F., Xu, J.P., Wei, J.C., Li, B.B., Shao, D.H., Shi, Y.Y., Qiu, Y.F., Ma, Z.Y., 2017. Doxycycline enhances adsorption and inhibits early-stage replication of porcine reproductive and respiratory syndrome virus in vitro. *Fems Microbiol Lett* 364.

Lucas, J., True, L., Hawley, S., Matsumura, M., Morrissey, C., Vessella, R., Nelson, P., 2008. The androgen-regulated type II serine protease TMPRSS2 is differentially expressed and mislocalized in prostate adenocarcinoma. *J Pathol* 215, 118-125.

Madeira, F., Park, Y.M., Lee, J., Buso, N., Gur, T., Madhusoodanan, N., Basutkar, P., Tivey, A.R.N., Potter, S.C., Finn, R.D., Lopez, R., 2019. The EMBL-EBI search and sequence analysis tools APIs in 2019. *Nucleic Acids Res* 47, W636-W641.

Maksimovic-Ivanic, D., Fagone, P., McCubrey, J., Bendtzen, K., Mijatovic, S., Nicoletti, F., 2017. HIV-protease inhibitors for the treatment of cancer: Repositioning HIV protease inhibitors while developing more potent NO-hybridized derivatives? *Int J Cancer* 140, 1713-1726.

Marberger, M., 2006. Drug Insight: 5 $\alpha$ -reductase inhibitors for the treatment of benign prostatic hyperplasia. *Nat Clin Pract Urol* 3, 495-503.

Marder, S.R., Kramer, M., Ford, L., Eerdeken, E., Lim, P., Eerdeken, M., Lowy, A., 2007. Efficacy and safety of paliperidone extended-release tablets: Results of a 6-week, randomized, placebo-controlled study. *Biol Psychiat* 62, 1363-1370.

Montes-Grajales, D., Puerta-Guardo, H., Espinosa, D.A., Harris, E., Caicedo-Torres, W., Olivero-Verbel, J., Martinez-Romero, E., 2020. In silico drug repurposing for the identification of potential candidate molecules against arboviruses infection. *Antiviral Res* 173, 104668.

Mortier, E., Pouchot, J., Vinceneux, P., Lalande, M., 2001. Ergotism related to interaction between nelfinavir and ergotamine. *Am J Med* 110, 594-594.

Mostaghel, E.A., Nelson, P.S., Lange, P., Lin, D.W., Taplin, M.E., Balk, S., Ellis, W., Kantoff, P., Marck, B., Tamae, D., Matsumoto, A.M., True, L.D., Vessella, R., Penning, T., Merrill, R.H., Gulati, R., Montgomery, B., 2014. Targeted Androgen Pathway Suppression in Localized Prostate Cancer: A Pilot Study. *J Clin Oncol* 32, 229-+.

Phillips, J.C., Braun, R., Wang, W., Gumbart, J., Tajkhorshid, E., Villa, E., Chipot, C., Skeel, R.D., Kale, L., Schulten, K., 2005. Scalable molecular dynamics with NAMD. *J Comput Chem* 26, 1781-1802.

Prajapat, M., Sarma, P., Shekhar, N., Avti, P., Sinha, S., Kaur, H., Kumar, S., Bhattacharyya, A., Kumar, H., Bansal, S., Medhi, B., 2020. Drug targets for corona virus: A systematic review. *Indian J Pharmacol* 52, 56-65.

Roehrborn, C.G., Boyle, P., Nickel, J.C., Hoefner, K., Andriole, G., Aria, A., Investigators, A.S., 2002. Efficacy and safety of a dual inhibitor of 5- $\alpha$ -reductase types 1 and 2 (dutasteride) in men with benign prostatic hyperplasia. *Urology* 60, 434-441.

Rosenthal, E., Sala, F., Chichmanian, R.M., Batt, M., Cassuto, J.P., 1999. Ergotism related to concurrent administration of ergotamine tartrate and indinavir. *JAMA* 281, 987.

Rothan, H.A., Buckle, M.J., Ammar, Y.A., Mohammadjavad, P., Shatrah, O., Noorsaadah, A.R., Rohana, Y., 2013. Study the antiviral activity of some derivatives of tetracycline and non-steroid anti inflammatory drugs towards dengue virus. *Trop Biomed* 30, 681-690.

Rothan, H.A., Mohamed, Z., Paydar, M., Abd Rahman, N., Yusof, R., 2014a. Inhibitory effect of doxycycline against dengue virus replication in vitro. *Arch Virol* 159, 711-718.

Rothan, H.A., Mohamed, Z., Paydar, M., Rahman, N.A., Yusof, R., 2014b. Inhibitory effect of doxycycline against dengue virus replication in vitro. *Arch Virol* 159, 711-718.

Scandella, E., Eriksson, K.K., Hertzog, T., Drosten, C., Chen, L., Gui, C., Luo, X., Shen, J., Shen, X., Siddell, S.G., Ludewig, B., Jiang, H., Gunther, S., Thiel, V., 2006. Identification and evaluation of coronavirus replicase inhibitors using a replicon cell line. *Adv Exp Med Biol* 581, 609-613.

Silberstein, S.D., 1997. The pharmacology of ergotamine and dihydroergotamine. *Headache* 37 Suppl 1, S15-25.

Smilack, J.D., 1999. The tetracyclines. *Mayo Clin Proc* 74, 727-729.

St John, S.E., Tomar, S., Stauffer, S.R., Mesecar, A.D., 2015. Targeting zoonotic viruses: Structure-based inhibition of the 3C-like protease from bat coronavirus HKU4-The likely reservoir host to the human coronavirus that causes Middle East Respiratory Syndrome (MERS). *Bioorgan Med Chem* 23, 6036-6048.

Su, S., Wong, G., Shi, W., Liu, J., Lai, A.C.K., Zhou, J., Liu, W., Bi, Y., Gao, G.F., 2016. Epidemiology, Genetic Recombination, and Pathogenesis of Coronaviruses. *Trends Microbiol* 24, 490-502.

Thiel, V., Ivanov, K.A., Putics, A., Hertzog, T., Schelle, B., Bayer, S., Weissbrich, B., Snijder, E.J., Rabenau, H., Doerr, H.W., Gorbalenya, A.E., Ziebuhr, J., 2003. Mechanisms and enzymes involved in SARS coronavirus genome expression. *Journal of General Virology* 84, 2305-2315.

Thomson, A., 2005. Dutasteride: an evidence-based review of its clinical impact in the treatment of benign prostatic hyperplasia. *Core Evid* 1, 143-156.

Tomar, S., Johnston, M.L., St John, S.E., Osswald, H.L., Nyalapatla, P.R., Paul, L.N., Ghosh, A.K., Denison, M.R., Mesecar, A.D., 2015. Ligand-induced Dimerization of Middle East Respiratory Syndrome (MERS) Coronavirus nsp5 Protease (3CLpro): IMPLICATIONS FOR nsp5 REGULATION AND THE DEVELOPMENT OF ANTIVIRALS. *J Biol Chem* 290, 19403-19422.

Trott, O., Olson, A.J., 2010. AutoDock Vina: improving the speed and accuracy of docking with a new scoring function, efficient optimization, and multithreading. *J Comput Chem* 31, 455-461.

Via, M.A., Chandra, H., Araki, T., Potenza, M.V., Skamagas, M., 2010. Bromocriptine approved as the first medication to target dopamine activity to improve glycemic control in patients with type 2 diabetes. *Diabetes Metab Syndr Obes* 3, 43-48.

WHO, 2020. WHO Director-General's remarks at the media briefing on 2019-nCoV on 11 February 2020 <https://www.who.int/dg/speeches/detail/who-director-general-s-remarks-at-the-media-briefing-on-2019-ncov-on-11-february-2020>.

Wu C, L.Y., Yang Y, Zhang P, Zhong W, Wang Y, Wang Q, Xu Y, Li M, Li X,, Zheng M, C.L., Li H, , 2020. Analysis of therapeutic targets for SARS-CoV-2 and discovery of potential drugs by computational methods. *Acta Pharmaceutica Sinica B*.

Wu C, L.Y., Yang Y, Zhang P, Zhong W, Wang Y, Wang Q, Xu Y, Li M, Li X,Zheng M, Chen L, Li H, , 2020. nalysis of therapeutic targets for SARS-CoV-2 and discovery of potential drugsby computational methods,. *Acta Pharmaceutica Sinica B* <https://doi.org/10.1016/j.apsb.2020.02.008>.

Wu, F., Zhao, S., Yu, B., Chen, Y.M., Wang, W., Song, Z.G., Hu, Y., Tao, Z.W., Tian, J.H., Pei, Y.Y., Yuan, M.L., Zhang, Y.L., Dai, F.H., Liu, Y., Wang, Q.M., Zheng, J.J., Xu, L., Holmes, E.C., Zhang, Y.Z., 2020. A new coronavirus associated with human respiratory disease in China. *Nature*.

Wu, Z.C., Wang, X., Wei, J.C., Li, B.B., Shao, D.H., Li, Y.M., Liu, K., Shi, Y.Y., Zhou, B., Qiu, Y.F., Ma, Z.Y., 2015. Antiviral activity of doxycycline against vesicular stomatitis virus in vitro. *Fems Microbiol Lett* 362.

Xu, X., Liu, Y., Weiss, S., Arnold, E., Sarafianos, S.G., Ding, J., 2003. Molecular model of SARS coronavirus polymerase: implications for biochemical functions and drug design. *Nucleic Acids Res* 31, 7117-7130.

Yamamoto, N., Yang, R.G., Yoshinaka, Y., Amari, S., Nakano, T., Cinatl, J., Rabenau, H., Doerr, H.W., Hunsmann, G., Otaka, A., Tamamura, H., Fujii, N., Yamamoto, N., 2004. HIV protease inhibitor nelfinavir inhibits replication of SARS-associated coronavirus. *Biochem Bioph Res Co* 318, 719-725.

Yu, X.J., Liang, M.F., Zhang, S.Y., Liu, Y., Li, J.D., Sun, Y.L., Zhang, L., Zhang, Q.F., Popov, V.L., Li, C., Qu, J., Li, Q., Zhang, Y.P., Hai, R., Wu, W., Wang, Q., Zhan, F.X., Wang, X.J., Kan, B., Wang, S.W., Wan, K.L., Jing, H.Q., Lu, J.X., Yin, W.W., Zhou, H., Guan, X.H., Liu, J.F., Bi, Z.Q., Liu, G.H., Ren, J., Wang, H., Zhao, Z., Song, J.D., He, J.R., Wan, T., Zhang, J.S., Fu, X.P., Sun, L.N., Dong, X.P., Feng, Z.J., Yang, W.Z., Hong, T., Zhang, Y., Walker, D.H., Wang, Y., Li, D.X., 2011. Fever with thrombocytopenia associated with a novel bunyavirus in China. *N Engl J Med* 364, 1523-1532.

Yuan, S., Chan, J.F., den-Haan, H., Chik, K.K., Zhang, A.J., Chan, C.C., Poon, V.K., Yip, C.C., Mak, W.W., Zhu, Z., Zou, Z., Tee, K.M., Cai, J.P., Chan, K.H., de la Pena, J., Perez-Sanchez, H., Ceron-Carrasco, J.P., Yuen, K.Y., 2017. Structure-based discovery of clinically approved drugs as Zika virus NS2B-NS3 protease inhibitors that potently inhibit Zika virus infection in vitro and in vivo. *Antiviral Res* 145, 33-43.

Zaki, A.M., van Boheemen, S., Bestebroer, T.M., Osterhaus, A.D.M.E., Fouchier, R.A.M., 2012. Isolation of a Novel Coronavirus from a Man with Pneumonia in Saudi Arabia. *New Engl J Med* 367, 1814-1820.

Zhou, P., Yang, X.L., Wang, X.G., Hu, B., Zhang, L., Zhang, W., Si, H.R., Zhu, Y., Li, B., Huang, C.L., Chen, H.D., Chen, J., Luo, Y., Guo, H., Jiang, R.D., Liu, M.Q., Chen, Y., Shen, X.R., Wang, X., Zheng, X.S., Zhao, K., Chen, Q.J., Deng, F., Liu, L.L., Yan, B., Zhan, F.X., Wang, Y.Y., Xiao, G.F., Shi, Z.L., 2020. A pneumonia outbreak associated with a new coronavirus of probable bat origin. *Nature*.

Ziebuhr, J., 2004. Molecular biology of severe acute respiratory syndrome coronavirus. *Curr Opin Microbiol* 7, 412-419.

Ziebuhr, J., 2005. The coronavirus replicase. *Curr Top Microbiol Immunol* 287, 57-94.

## Figure Legends

**Figure 1:** Outline of the study.

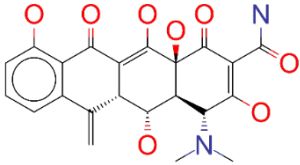
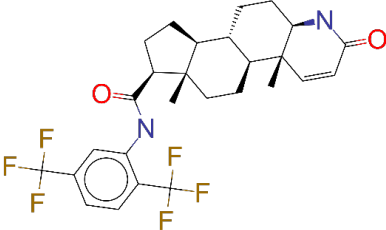
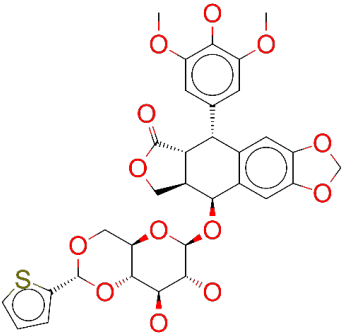
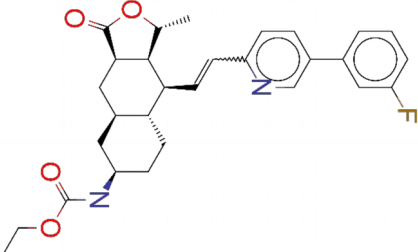
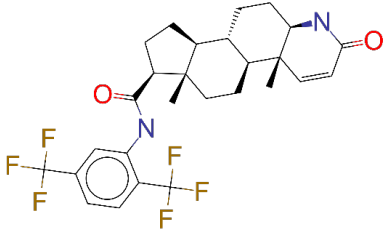
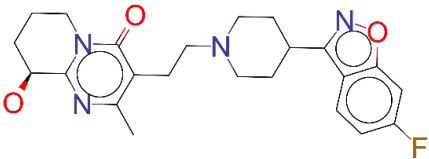
**Figure 2:** The structure of 3 chymotrypsin like protease (3CL<sup>pro</sup>) **A)** Catalytic pocket of SARS-CoV-2 of 3CL<sup>pro</sup> is shown in red. Protein is shown in white cartoon (left) or surface (right) (PDB ID: 6y84). Catalytic residues His<sup>41</sup> and Cys<sup>145</sup> are shown with sticks (red) representation. **B)** Sequence alignment of 3CL<sup>pro</sup> from SARS-CoV, MERS, HKU and SARS-CoV2 viruses. Conserved residues are highlighted in red. Arrows show the conserved residues (His41 and Cys145) which are critical for the protease activity. **C)** Superimposing the crystal structures of 3CL<sup>pro</sup> from SARS shown in cyan (PDB ID: 3VB3), MERS shown in green (PDB ID: 4ylu), HKU4 shown in navy (PDB ID: 4yo9) and SARS-CoV-2 shown in white (PDB ID: 6y84) cartoon (left) or surface representations (right). Conserved catalytic residues (His<sup>41</sup> and Cys<sup>145</sup>) are shown in red stick representation.

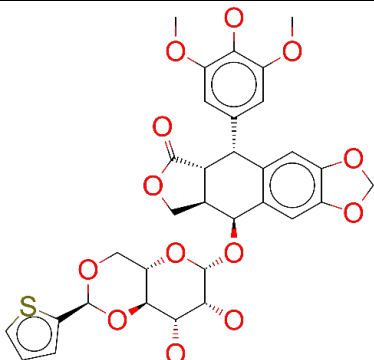
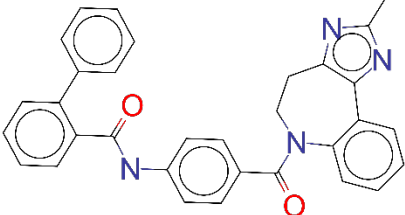
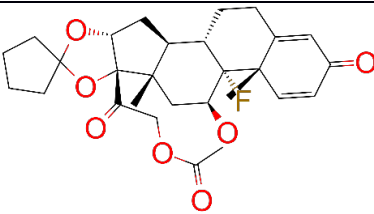
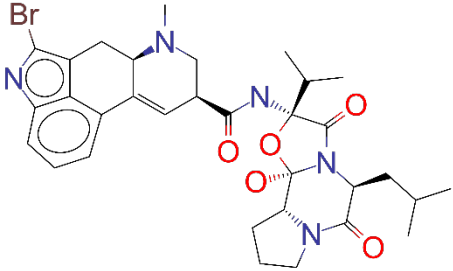
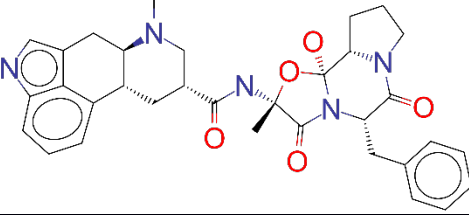
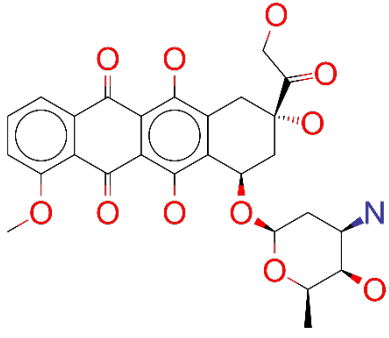
**Figure 3:** The structure of RNA-dependent RNA polymerase (RdRp) **A)** RdRp is shown in blue cartoon (top) or surface representations (below), binding partners nsp8 are nsp7 are shown in orange and cyan cartoon, respectively (PDB ID:6nur). **B)** Sequence alignment of RdRp from SARS and SARS-CoV2. Conserved residues are highlighted in red. Residues interacting with nsp8 are indicated with rectangle boxes.

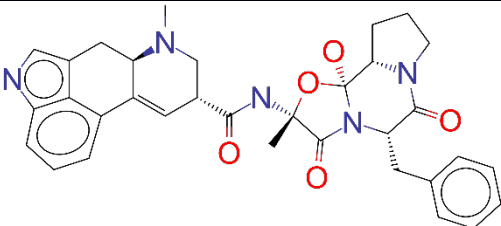
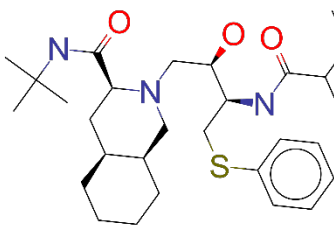
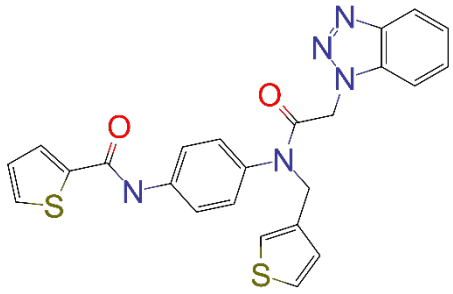
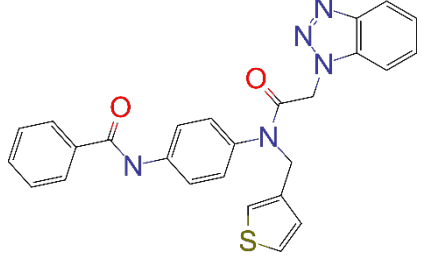
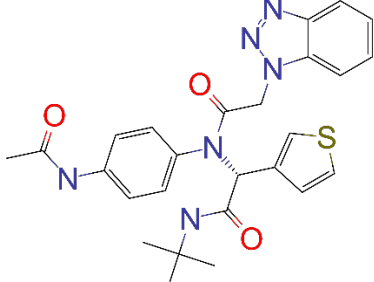
**Figure 4:** Binding mode of top 4 candidates drugs to SARS-CoV-2 3CL<sup>pro</sup>. **A)** tetracycline **B)** dihydroergotamine **C)** dutastride, **D)** nelfinavir, and **E)** paliperidone. Proteins are shown in ribbon and drugs are shown with stick representations at left panels for each drug. Molecular simulations were performed and the frequency of interacting amino acid residues are shown in middle panels. Right panel shows the amino acid residues of the SARS-CoV-2 3CL<sup>pro</sup> that interacts with drugs after molecular simulations. The following coloring scheme is used in figures: carbons are white, nitrogens are blue, oxygens are red, sulphurs are yellow, however, carbons in ligands are shown in cyan.

**Figure 5:** Binding mode of top 4 candidates drugs to RdRp. **A)** ergotamine **B)** eltrombopag **C)** conivaptan and **D)** tipranavir. Proteins are shown in ribbon and drugs are shown with stick representations at left panels for each drug. Molecular simulations were performed and the frequency of interacting amino acid residues are shown in middle panels. Right panel shows the amino acid residues of the SARS-CoV-2 3CL<sup>pro</sup> that interacts with drugs after molecular simulations. The following coloring scheme is used in figures: carbons are white, nitrogens are blue, oxygens are red, sulphurs are yellow, however, carbons in ligands are shown in cyan.

**Table 1:** List of top 15 drugs having the best binding affinity to SARS-CoV-2 3CL<sup>pro</sup> and 3CL<sup>pro</sup> inhibitors from MERS-CoV.

ZINC ID and/or Drug Name	2D Structure	Vina Binding Affinity (kcal/mol)	Pharmacology / Indication
ZINC000084480349 / Metacycline		-9.1	For the treatment of acute bacterial exacerbations of chronic bronchitis
ZINC000001612996 / Irinotecan		-9.1	For the treatment of metastatic colorectal cancer
ZINC000003932831 / Dutasteride		-8.9	Indicated for the treatment of symptomatic benign prostatic hyperplasia (BPH) in men with an enlarged prostate gland
ZINC000004099009 / Teniposide		-8.9	Teniposide is used for the treatment of refractory acute lymphoblastic leukaemia
ZINC000003925861 / Vorapaxar		-8.9	Vorapaxar is indicated for the reduction of thrombotic cardiovascular events in patients with a history of myocardial infarction or peripheral arterial disease
ZINC000003938684 / Etoposide		-8.9	For use in combination with other chemotherapeutic agents in the treatment of refractory testicular tumors
ZINC000004214700 / Paliperidone		-8.8	Used in the treatment of schizophrenia

ZINC000003831508 / Teniposide	 <p>The structure of Teniposide is a complex polycyclic molecule. It features a central decalin-like ring system with a fused benzene ring. Attached to this system are a 3,4,5-trimethoxyphenyl group, a 2-thienylmethyl group, and a 2,3-dihydro-2H-benzofuran ring system. Stereochemistry is indicated with wedges and dashes.</p>	-8.8	Teniposide is used for the treatment of refractory acute lymphoblastic leukaemia
ZINC000012503187 / Conivaptan	 <p>The structure of Conivaptan consists of two benzamide-like moieties connected by a central benzene ring. One amide group is attached to a phenyl ring, and the other is attached to a 2,3,4-trimethyl-1H-indazole ring system.</p>	-8.7	For the treatment of euvoletic or hypovolemic hyponatremia in hospitalized patients
ZINC000003977777 / Amsinonid	 <p>The structure of Amsinonid is a complex polycyclic molecule with a central decalin-like ring system. It features a cyclopentane ring fused to one of the decalin rings, a fluorine atom, and a carboxylic acid group. Stereochemistry is indicated with wedges and dashes.</p>	-8.7	Shows anti-inflammatory activity
ZINC000059364574 / Bromocriptine	 <p>The structure of Bromocriptine features a 6-bromo-2,3,4,5-tetrahydro-1H-indole ring system. It is connected via a methylene group to a piperazine ring, which is further substituted with a methyl group and a 2,3-dimethylbutyl group.</p>	-8.6	For the treatment of galactorrhea due to hyperprolactinemia, prolactin-dependent menstrual disorders and infertility, prolactin-secreting adenomas, prolactin-dependent male hypogonadism
ZINC000003978005 / Dihydroergotamine	 <p>The structure of Dihydroergotamine is a complex polycyclic molecule with a central ergoline-like ring system. It features a bromine atom, a methyl group, and a 2-phenylethyl group. Stereochemistry is indicated with wedges and dashes.</p>	-8.6	For the acute treatment of migraine headaches with or without aura and the acute treatment of cluster headache episodes.
ZINC000003830729/ Doxorubicin	 <p>The structure of Doxorubicin is a complex polycyclic molecule with a central tetracyclic ring system. It features a 14-hydroxy group, a 2,3-dihydro-2H-benzofuran ring system, and a 2,3,5-trimethoxyphenyl group. Stereochemistry is indicated with wedges and dashes.</p>	-8.6	Doxorubicin is used to produce regression in disseminated neoplastic conditions like acute lymphoblastic leukemia, acute myeloblastic leukemia, Wilms' tumor, neuroblastoma, soft tissue and bone sarcomas, breast carcinoma, ovarian carcinoma etc.

ZINC000052955754 / Ergotamine		-8.6	For use as therapy to abort or prevent vascular headache
ZINC000003833846/ Nelfinavir		-8.6	Used in combination with other antiviral drugs in the treatment of HIV in both adults and children
4F4		-7.5	
RFM		-7.5	Inhibitor of 3CL in MERS
4F5		-7.0	

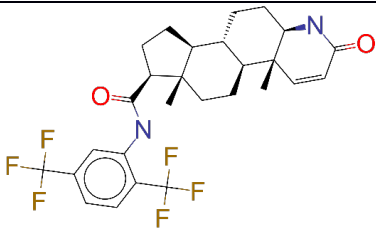
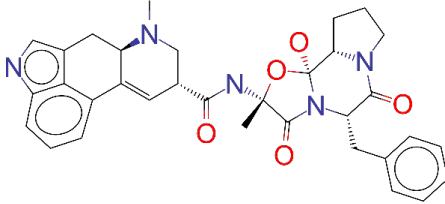
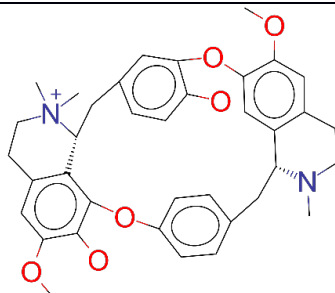
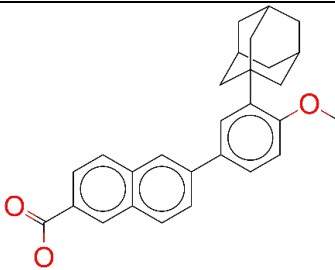
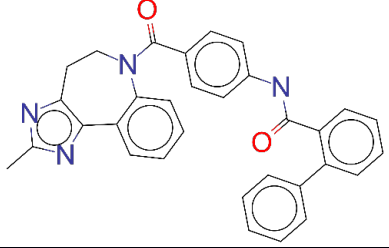
**Table 2:** Interacting residues of selected drugs with 3CL<sup>Pro</sup>

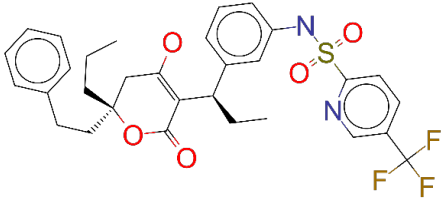
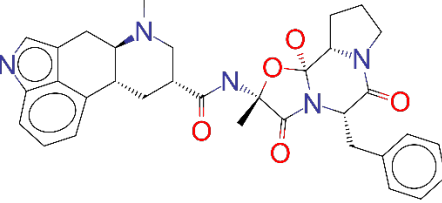
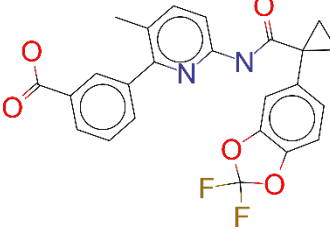
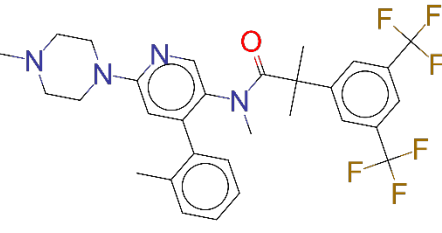
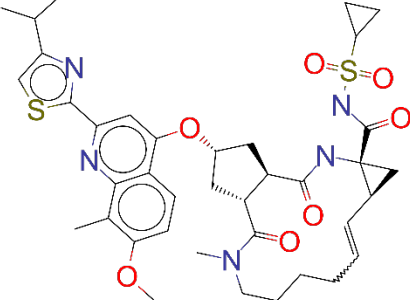
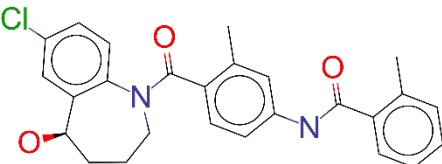
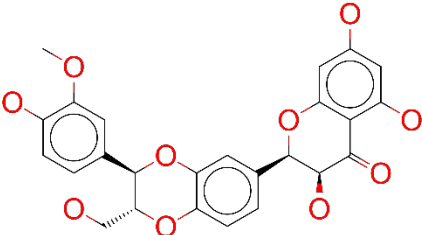
Drug	Interacting residues
Tetracycline	Thr26, His41, Cys45, Ser46, Met49, Asn142, Met165, Glu166, Gln189
Dihydroergotamine	Thr25, Thr26, His41, Thr45, Ser46, Met49, Gly143, Cys145
Dutasteride	Thr25, His41, Ser46, Asn142, Cys145, Glu166, Pro168, Gln189
Nelfinavir	Thr25, His41, Ser46, Leu141, Asn142, Gly143, Ser144, Cys145, Glu166, Pro168, Gln189
Paliperidone	Thr25, His41, Ser46, Leu141, Gly143, Cys145, Glu166, Gln189

**Table 3:** MM/GBSA Binding free energy of protease inhibitors and promising drugs to interfere with SARS-CoV-2 3CL<sup>pro</sup> and RdRp activities.

3Clpro		RdRp	
Drug Name	MM/ GBSA Binding free energy (kcal/mol)	Drug Name	MM/ GBSA Binding free energy (kcal/mol)
Tetracycline	-15.19 ± 2.76	Ergotamine	-24.65 ± 3.93
Dihydroergotamine	-16.22 ± 5.41	Eltrombopag	-35.33 ± 3.48
Dutasteride	-20.47 ± 6.29	Conivaptan	-23.83 ± 5.43
Nelfinavir	-26.28 ± 4.48	Tipranavir	-26.08 ± 3.86
Paliperidone	-18.23 ± 4.17		
4F4	-16.71 ± 4.66		
4F5	-24.96 ± 3.63		

**Table 4:** List of top 15 drugs having the best binding affinity to RdRp.

ZINC ID and/or Drug Name	2D Structure	Vina Binding Affinity (kcal/mol)	Clinical Trial
ZINC000003932831 / Dutasteride		-9.9	Indicated for the treatment of symptomatic benign prostatic hyperplasia (BPH) in men with an enlarged prostate gland
ZINC000052955754 / Ergotamine		-9.8	For use as therapy to abort or prevent vascular headache
ZINC000004198852 / d-Tubocurarine		-9.5	Used as a diagnosis agent for myasthenia gravis, and also to facilitate the intubation after induction of anesthesia in surgical procedure. No trial
ZINC000003784182 / Differin		-9.5	For the topical treatment of comedo, papular and pustular acne (acne vulgaris) of the face, chest or back.
ZINC000011679756 / Eltrombopag		-9.5	Thrombopoietin receptor agonists are pharmaceutical agents that stimulate platelet production in the bone marrow
ZINC000012503187 / Conivaptan		-9.4	For the treatment of euvolemic or hypovolemic hyponatremia in hospitalized patients

ZINC000100016058 / Tipranavir		-9.3	For combination antiretroviral treatment of HIV-1 infected adult patients with evidence of viral replication, who are highly treatment-experienced or have HIV-1 strains resistant to multiple protease inhibitors
ZINC000003978005 / Dihydroergotamine		-9.3	For the acute treatment of migraine headaches with or without aura and the acute treatment of cluster headache episodes
ZINC000064033452 / Lumacaftor		-9.3	lumacaftor is indicated for the treatment of cystic fibrosis (CF) in patients age 6 years and older who are homozygous for the F508del mutation in the CFTR gene.
ZINC000011681563 / Netupitant		-9.2	for use in combination with palonosetron for the prevention of acute and delayed vomiting and nausea associated with cancer chemotherapy including highly emetogenic chemotherapy
ZINC000253632968 / Simeprevir		-9.2	Indicated for the treatment of adults with chronic hepatitis C virus (HCV) infection:
ZINC000000538658 / Tolvaptan		-9.2	Treatment of symptomatic and resistant to fluid restriction euvolemic or hypervolemic hyponatremia associated with congestive heart failure, and cirrhosis.
ZINC000001757652 / Silibinin		-9.2	Currently being tested as a treatment of severe intoxications with hepatotoxic substances



**Table 5:** Interacting residues of selected drugs with RdRp

Drug	Interacting residues
Ergotamine	Leu270, Thr324, Phe326, Val330, Ala379, Val398
Eltrombopag	Tyr273, Val329, Val330, Arg331, Val398
Conivaptan	Leu270, Leu271, Tyr273, Thr324, Phe326, Leu329, Val330, Val398, Val675
Tipranavir	Leu270, Leu271, Tyr273, Thr324, Leu329, Val330, Arg331, Ala379, Phe396, Val398, Met666

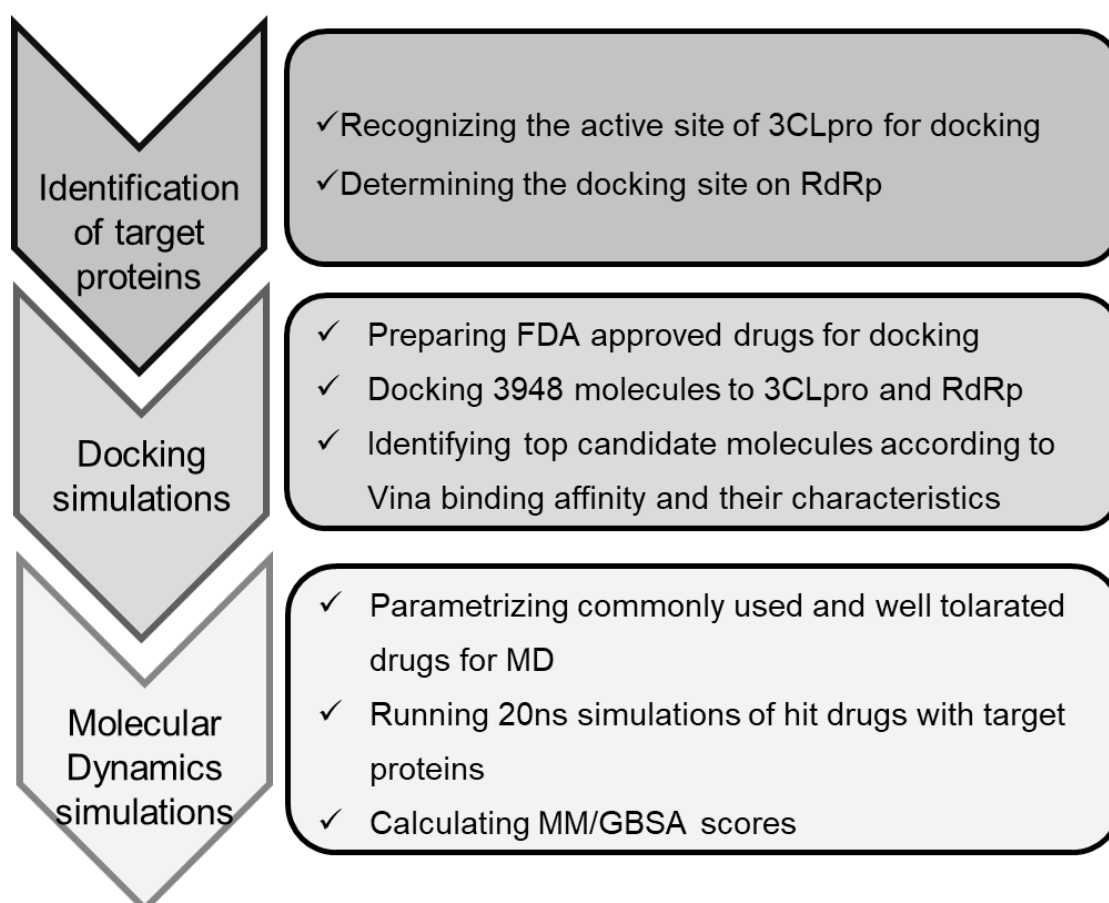


## Figure 1

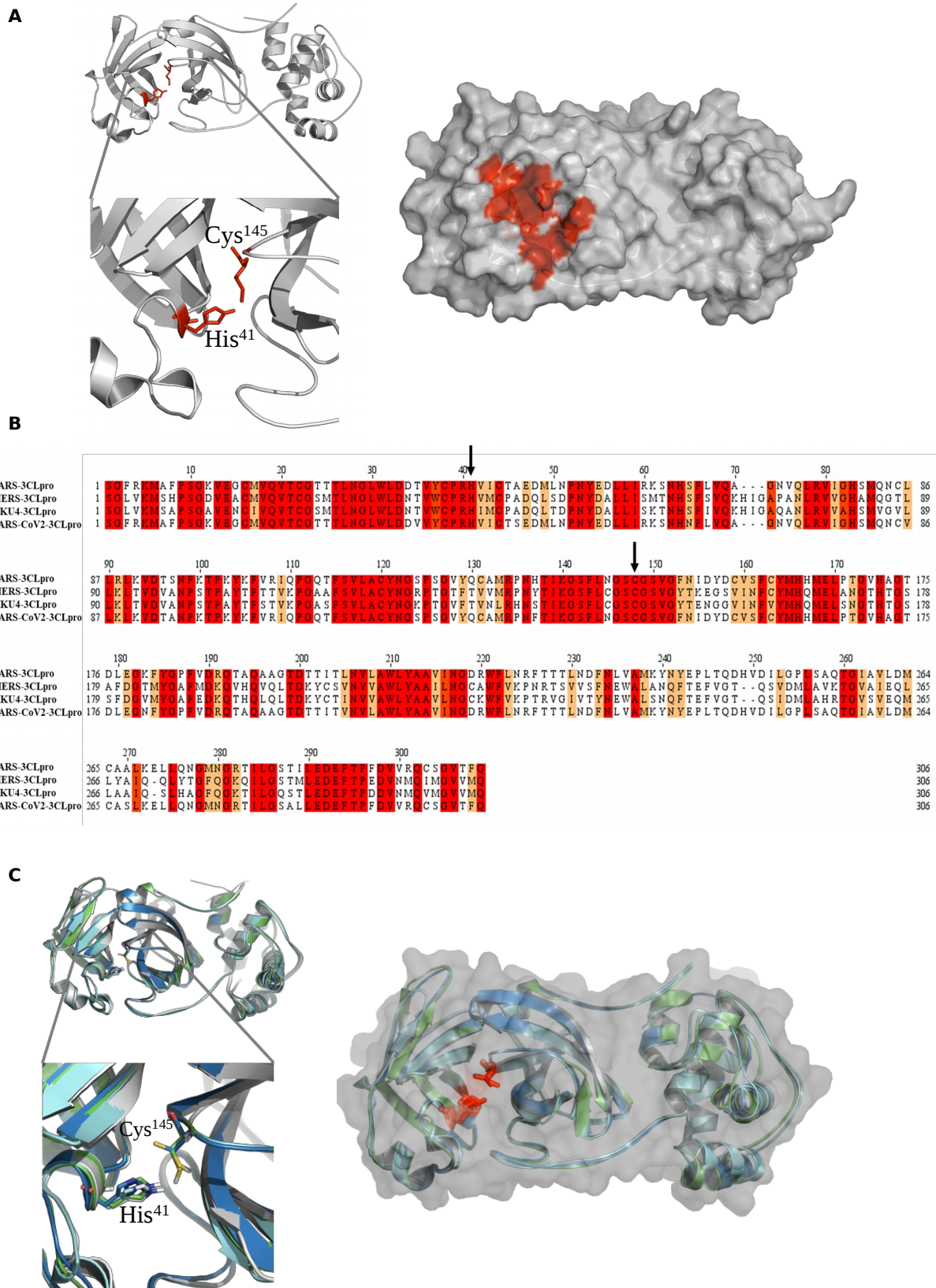
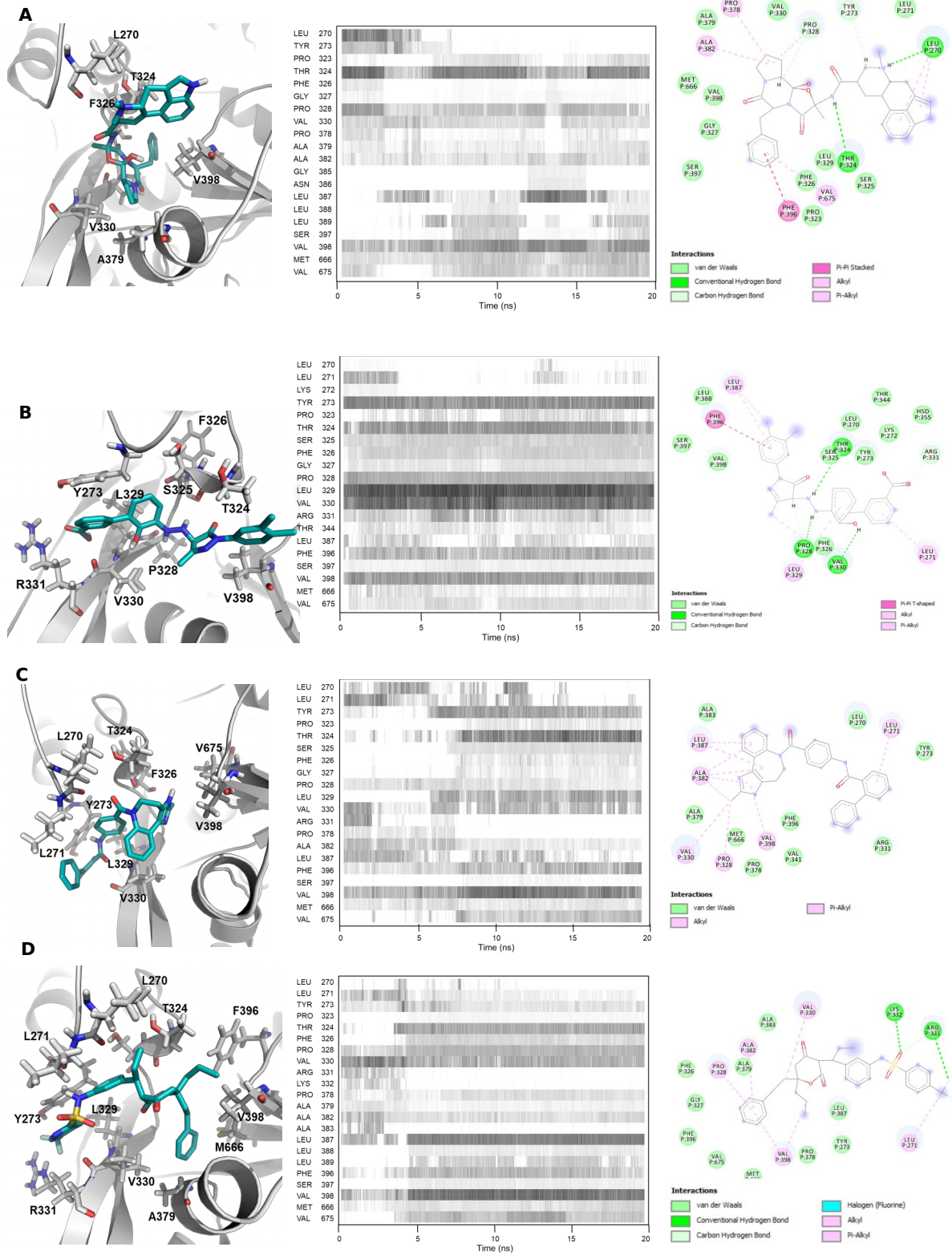


Figure 2







**Figure 5**

**Table S1:** Top 100 molecules having the best binding affinity to SARS-CoV-2 3CL<sup>Pro</sup>

ZINC ID	Vina Binding Affinity (kcal/mol)	Drug Name
ZINC000118917794	-9.3	
ZINC000001612996	-9.1	Irinotecan
ZINC000084480349	-9.1	Metacycline
ZINC000003932831	-8.9	Dutasteride
ZINC000003938684	-8.9	Etoposide
ZINC000003925861	-8.9	Vorapaxar
ZINC000004099009	-8.9	Teniposide
ZINC000004214700	-8.8	Paliperidone
ZINC000012503187	-8.7	Conivaptan
ZINC000003977777	-8.7	Amsinonid
ZINC000059364574	-8.6	Bromocriptine
ZINC000003978005	-8.6	Dihydroergotamine
ZINC000003830729	-8.6	Doxorubicin
ZINC000003830729	-8.6	Epirubicin
ZINC000052955754	-8.6	Ergotamine
ZINC000003977978	-8.6	Fluocinonide
ZINC000003833846	-8.6	Nelfinavir
ZINC000118917543	-8.6	Proscillaridin
ZINC000003978083	-8.6	Tubocurarin
ZINC000003927200	-8.6	Drospirenon
ZINC000003830431	-8.5	Cefoperazone
ZINC000003830629	-8.5	Danazol
ZINC000003830634	-8.5	Daunorubicin
ZINC000014210642	-8.5	Azilsartan
ZINC000003830816	-8.5	Etoposide
ZINC000064033452	-8.5	Lumacaftor
ZINC000035947015	-8.5	Oxytetracycline
ZINC000000538312	-8.5	Risperdone
ZINC000118917793	-8.5	-
ZINC000003830554	-8.5	-
ZINC000004172334	-8.4	Algestone acetophenide
ZINC000003915154	-8.4	Ciclesonide
ZINC000003977981	-8.4	Flucinolone
ZINC000118912562	-8.4	Dehydrocholic acid
ZINC000100003902	-8.4	Maraviroc
ZINC000100016058	-8.4	Tipranavir
ZINC000070466416	-8.3	Cabozantinib

ZINC000019701769	-8.3	Chlortetracycline
ZINC000003830332	-8.3	E155
ZINC000003830923	-8.3	Idarubicin
ZINC000000537877	-8.3	Ketanserin
ZINC000003831119	-8.3	Mezlocillin
ZINC000004175630	-8.3	Pimozide
ZINC000003938686	-8.3	Palbociclib
ZINC000003831614	-8.3	Zeranol
ZINC000253632968	-8.3	Simeprevir
ZINC000064220355	-8.3	Ursodeoxycholic acid
ZINC000003810860	-8.3	Ezetimibe
ZINC000035051264	-8.3	-
ZINC000003830632	-8.3	-
ZINC000003830732	-8.3	-
ZINC000118912449	-8.2	6-methylprednisolone
ZINC000003782818	-8.2	Candesartan
ZINC000003830403	-8.2	Cefatrizine
ZINC000021981454	-8.2	Clocortolone
ZINC000016052277	-8.2	Doxycycline
ZINC000011679756	-8.2	Eltrombopag
ZINC000003830845	-8.2	Flucloxacillin
ZINC000004097305	-8.2	Flunisolide
ZINC000118912517	-8.2	Fluorometholone
ZINC000001482077	-8.2	Gliquidone
ZINC000004212851	-8.2	Desonide
ZINC000006304550	-8.2	Prednisolon
ZINC000003938746	-8.2	Reserpine
ZINC000169621200	-8.2	Rifaximin
ZINC000057678901	-8.2	Rolitetraacycline
ZINC000003914596	-8.2	Saquinavir
ZINC000002033590	-8.2	Silibinin
ZINC000001542113	-8.2	Vilazodone
ZINC000035051264	-8.2	-
ZINC000004744093	-8.2	-
ZINC000118913190	-8.2	-
ZINC000003830260	-8.1	Azlocillin
ZINC000001996117	-8.1	Darifenacin
ZINC000003830769	-8.1	Estradiol benzoate
ZINC000098052857	-8.1	-
ZINC000006716957	-8.1	Nilotinib
ZINC000118913751	-8.1	Pancuronium
ZINC000003831344	-8.1	Piperacillin
ZINC000005752191	-8.1	Diflorasone
ZINC000001530886	-8.1	Telmisartan
ZINC000084441937	-8.1	Tetracycline
ZINC000085555528	-8.1	Vinblastine

ZINC000000538550	-8.1	Ziprasidone
ZINC000028630683	-8.1	-
ZINC000001530603	-8.1	Cloxacillin
ZINC000018516586	-8.1	Delavirdine
ZINC000058581064	-8.1	Dolutegravir
ZINC000003830427	-8.1	Cefonicid
ZINC000003831241	-8.1	Oxacillin
ZINC000003831234	-8.1	Novobiocin
ZINC000085555528	-8.1	Vinblastine
ZINC000118916776	-8.1	Methylprednisolone hemisuccinate
ZINC000003872931	-8	Irbesartan
ZINC000000968277	-8	Troglitazone
ZINC000004428527	-8	Desoxycortisone
ZINC000011617039	-8	Pazopanib
ZINC000000601229	-8	Azelastine
ZINC000003977990	-8	Fludrocortisone
ZINC000066166864	-8	Alectinib

**Table S2:** Top 100 molecules having the best binding affinity to RdRp

ZINC ID	Vina Binding Affinity (kcal/mol)	Drug Name
ZINC000003932831	-9.9	Dutasteride
ZINC000052955754	-9.8	Ergotamine
ZINC000004198852	-9.5	d-Tubocurarine
ZINC000003784182	-9.5	Differin
ZINC000011679756	-9.5	Eltrombopag
ZINC000012503187	-9.4	Conivaptan
ZINC000100016058	-9.3	Tipranavir
ZINC000003978005	-9.3	Dihydroergotamine
ZINC000064033452	-9.3	Lumacaftor
ZINC000011681563	-9.2	Netupitant
ZINC000253632968	-9.2	Simeprevir
ZINC000000538658	-9.2	Tolvaptan
ZINC000001757652	-9.2	Silibinin
ZINC000059364577	-9.2	-
ZINC000001550477	-9.2	Lapatinib
ZINC000001542113	-9.2	Vilazodone
ZINC000059364572	-9.2	-
ZINC000059364574	-9.2	-
ZINC000053683151	-9.2	Bromocriptine
ZINC000003831509	-9.2	Teniposide
ZINC000003978083	-9.2	Tubocurarin
ZINC000001612996	-9.2	Irinotecan
ZINC000001996117	-9.1	Darifenacin
ZINC000003816514	-9.1	Rolapitant
ZINC000006716957	-9.1	Nilotinib
ZINC000085537014	-9.1	Cobicistat
ZINC000004175630	-9.1	Primozone
ZINC000100003902	-9.1	Maraviroc
ZINC000058581064	-9.1	Dolutegravir
ZINC000059364575	-9.1	-
ZINC000000607700	-9.1	-
ZINC000004172334	-9.1	Algestone acetophenide
ZINC000003830772	-9	Estradiol cypionate
ZINC000001530788	-9	Cromolyn
ZINC000004099009	-9	Teniposide
ZINC000003831511	-9	Terfenadine
ZINC000003915154	-9	Ciclesonide
ZINC000003977777	-9	Amsinonid
ZINC000001482077	-9	Gliquidone
ZINC000003872566	-9	Fexofenadine
ZINC000022448696	-9	Indinavir
ZINC000118915484	-9	-

ZINC000000538550	-8.9	Ziprasidone
ZINC000118917543	-8.9	-
ZINC000003914596	-8.9	Saquinavir
ZINC000059364577	-8.9	-
ZINC000008577218	-8.9	Folic acid
ZINC000003925861	-8.9	Vorapaxar
ZINC000001999441	-8.9	Nebivolol
ZINC000022010649	-8.9	Panobinostat
ZINC000000601317	-8.9	Difenoxin
ZINC000035801098	-8.9	Indacaterol
ZINC000008585850	-8.9	-
ZINC000118916775	-8.8	-
ZINC000000538312	-8.8	Risperidon
ZINC000049036447	-8.8	Suvorexant
ZINC000003927822	-8.8	Lurasidone
ZINC000000537804	-8.8	Glisoxepide
ZINC000094566092	-8.8	Doxazosin
ZINC000001529323	-8.8	Methotrexate
ZINC000052716421	-8.8	Flibanserin
ZINC000003936683	-8.8	Solifenacin
ZINC000004198845	-8.7	-
ZINC000000897408	-8.7	Bicalutamide
ZINC000169621200	-8.7	Rifaximin
ZINC000068153186	-8.7	Dabrafenib
ZINC000084758479	-8.7	Greppiprazole
ZINC000098052857	-8.7	-
ZINC000003830627	-8.7	-
ZINC000000537795	-8.7	Glipizide
ZINC000118917794	-8.7	-
ZINC000003802417	-8.7	Alvimopan
ZINC000019796080	-8.7	Inapsine
ZINC000019632618	-8.7	Imatinib
ZINC000118913742	-8.7	Vecuronium
ZINC000002036732	-8.7	Florantyrone
ZINC000019632891	-8.7	Cinnarizine
ZINC000001530886	-8.6	Telmisartan
ZINC000059364577	-8.6	-
ZINC000004214700	-8.6	Paliperidone
ZINC000043207238	-8.6	Canagliflozin
ZINC000066166864	-8.6	Alectinib
ZINC000000537877	-8.6	Ketanserin
ZINC000004340355	-8.6	
ZINC000034608502	-8.6	Umeclidinium
ZINC000003810860	-8.6	Ezetimibe
ZINC000012504271	-8.6	Atovaquone proguanil hydrochloride
ZINC000000538505	-8.6	Trifluperidol

ZINC000003830839	-8.6	Finasteride
ZINC000035902489	-8.6	Crizotinib
ZINC000003881958	-8.6	Danol
ZINC000003830826	-8.5	Fazadinium
ZINC000059364574	-8.5	-
ZINC000070466416	-8.5	Cabozantinib
ZINC000068202099	-8.5	Erismodegib
ZINC000118915483	-8.5	-
ZINC000001536109	-8.5	-
ZINC000019364226	-8.5	Buclizine
ZINC000003831151	-8.5	Montelukast
ZINC000118917544	-8.5	Proscillaridin

**Table S3:** List of common drugs among top 100 molecules having the best binding affinities to SARS-CoV-2 3CL<sup>pro</sup> and RdRp

Common Drugs
Algestone acetophenide
Alvesco
Dutasteride
Cabozantinib
Conivaptan
Amsinonide
Darifenacin
Dihydroergotamine
Dolutegravir
Eltrombopag
Ergotamine
Gliquidone
Irinotecan
Ketanserin
Lumacaftor
Maraviroc
Nilotinib
Orap
Paliperidone
Proscillaridin
Rifaximin
Risperidone
Saquinavir
Silibinin
Simeprevir
Telmisartan
Teniposide
Tipranavir
Tubocurarin
Vilazodone
Vorapaxar
Teniposide
Ezetimibe
Ziprasidone

## Supplementary Figure Legends

**Figure S1:** Histogram of Vina binding affinity (kcal/mol) distribution of drugs to A) SARS-CoV-2 3CL<sup>pro</sup> and B) RdRp

**Figure S2:** Binding mode of top inhibitors of SARS-CoV 3CL<sup>pro</sup> against SARS-CoV-2 3CL<sup>pro</sup>. **A)** 4f4 **B)** 4f5. Molecular simulations were performed and the frequency of interacting amino acid residues are shown in top panels. Bottom panel shows the amino acid residues of the SARS-CoV-2 3CL<sup>pro</sup> that interacts with inhibitors after molecular simulations.

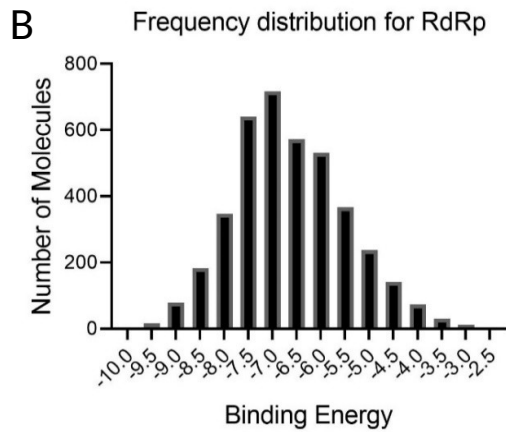
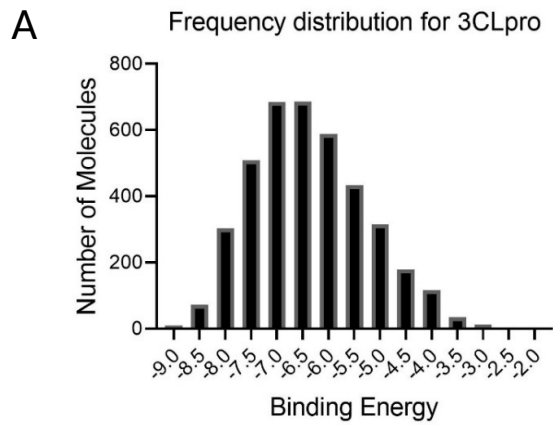
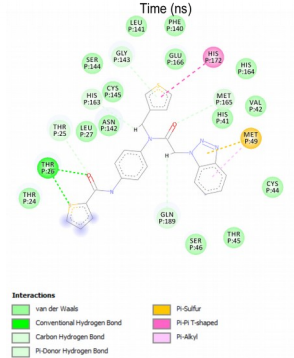
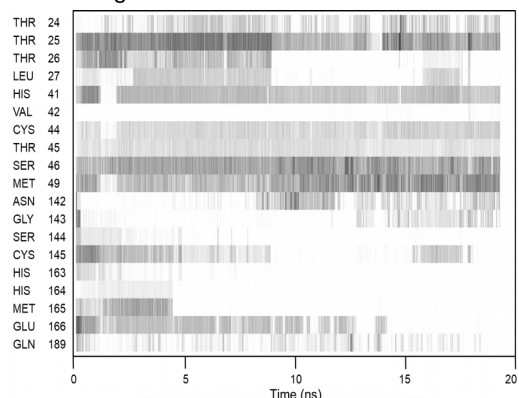


**Figure S1**

### Protein-ligand interaction for 4f4-3CLPro



### Protein-ligand interaction for 4f5-3CLPro

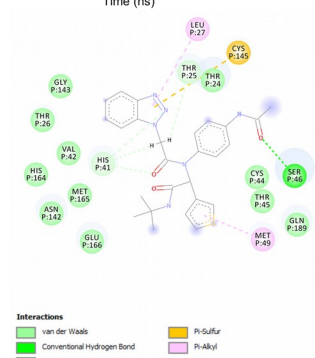
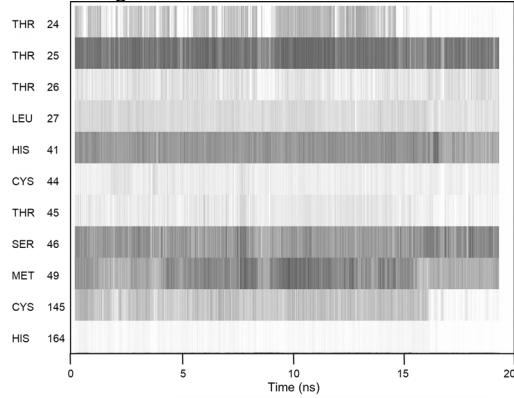


**Figure S2**